Manuscript Details

Manuscript number	OE_2018_807_R1
Title	Hydrodynamic responses and power efficiency analyses of an oscillating wave surge converter under different simulated PTO strategies
Article type	Research paper

Abstract

Experimental investigation on the power performance of a bottom hinged oscillating wave surge converters (OWSC) with different power take-off (PTO) damping strategies are conducted in regular and irregular waves. The hydrodynamic performance of the OWSC under different damping modes, in regular waves and irregular waves, is observed. For regular waves, the effects of the main influential parameters (including the incident wave height, wave frequency, phase difference between the buoy velocity and wave elevation) on the output power were quantitatively studied. Six damping coefficients of the linear PTO damping is examined under constant incident wave height, and increasing wave frequencies and an output power curve along wave frequency are presented for each input gain of the PTO simulation platform in both linear damping mode and nonlinear damping mode. Additionally, the best coefficient or input gain is obtained for both linear or nonlinear PTO damping mode in different wave conditions. The phase difference between the buoy velocity and wave elevation of the OWSC model in irregular waves has the same trend as that in regular waves. The output electricity in the JONSWAP spectrum is found to be (approximately 300%) higher than that in a user-defined spectrum for the same wave parameters.

Keywords	Model testing, Oscillating type wave converter, Hydrodynamic responses, Output power curves, Different PTO strategies
Taxonomy	Ocean Engineering, Renewable Energy
Manuscript category	Ocean Engineering

Corresponding Author	Xue Jiang
Order of Authors	Xue Jiang, Alexander Day, David Clelland
Suggested reviewers	Jiawang Chen, Fang He, Ming Li

Submission Files Included in this PDF

File Name [File Type]

Cover Letter-XJ.docx [Cover Letter]

response to reviewer-WEC2.docx [Response to Reviewers]

manuscript of WEC2- revision.docx [Manuscript File]

To view all the submission files, including those not included in the PDF, click on the manuscript title on your EVISE Homepage, then click 'Download zip file'.

Room 216, Henry Dyer Building
100 Montrose Street
Glasgow
G4 0LZ
Scotland, UK

14th August 2018

Dear Editor,

Submission of the two companied papers “An innovative generic platform to simulate PTO damping for ocean energy converters based on SIL method” and “Hydrodynamic response and power efficiency analyses of the oscillating wave surge converter with different simulated PTO strategies” authored by Xue Jiang, Sandy Day, David Clelland.

I would like to submit the enclosed manuscripts entitled “An innovative generic platform to simulate PTO damping for ocean energy converters based on SIL method” and “Hydrodynamic response and power efficiency analyses of the oscillating wave surge converter with different simulated PTO strategies” separately, but it may require you to arrange the two papers to the same reviewers. And we are very thankful for your consideration to publish them in the Journal of Ocean Engineering.

In the first paper, we propose a generic PTO (power-take- off) simulation platform which can be used to predict how devices perform in real conditions when a simulated linear or non-linear PTO damping is employed. Numerous calibrating tests are carried out to characterize it and draw the uncertainty of it. General relationships between damping coefficients and input gains of the platform are also drawn.

In the second paper, a 40th scaled Oyster device is applied on this platform, numerous tank tests in both regular and irregular waves with linear or nonlinear PTO damping strategies are carried out. Hydrodynamic performance and power efficiency analyses of the OWSC under different PTO strategies are drawn.

I would also like to declare that the work is original and it has not been published previously or not under consideration for publication elsewhere. All the authors listed have approved the manuscript enclosed to be submitted.

I sincerely hope that you could consider this work favourably.
Yours sincerely,

Xue Jiang, PhD Student
Department of Naval Architecture, Ocean and Marine Engineering
University of Strathclyde
E-mail: xue.jiang@strath.ac.uk
Telephone: +44(0)7563954354

Response to reviewer 1

1. The importance of nonlinear damping and necessity for the investigation on nonlinear damping effects are not demonstrated in detail enough.

   Yes, thanks a lot for the comment. And some related demonstration has been added in the section of introduction.

2. It is advised to integrate the introduction section and literature review section, since the novelty should be stated after the recent literatures are well reviewed.

   Yes, have done.

3. In lines 144 in pages 4, the ITTC's full name should be given.

   Yes, has done.

4. In pages 19-21, some references give all the authors' name, while the others' only give the first author's name. All the author's name in the References the should be given clearly.

   Yes. has rechecked to assure that all authors' names are properly listed.

Response to reviewer 2

1. Technical part

1. The highlights 2-4 in lines 27-32 are unnecessarily listed on page 1.

   - Yes, highlights 2-4 have been removed and one highlight' The best PTO damping strategy and the corresponding input gains have been achieved and attached.' is added.

2. A previous paper mentioned in lines 42-44 should be put in the reference section if it was published. If it was not published, please remove it from the paper.

devices do not perform as well as might be expected. A PTO simulation platform is proposed in the previous paper – "A Novel Experimental Platform with Simulated PTO for Ocean Energy Converters based on SIL Method", in which a generic approach to simulate PTO damping has been calibrated.

The previous paper mentioned has been put in the reference section as a manuscript.

3. In line 117, please write the complete response to the system driven by $F_0 \sin \omega t$. The response simply in the form $x(t) = X/2\sin(\omega t - \pi/2 + \beta)$ is not enough. It will be better to cite references, e.g., [1-3], for the complete response to a system.

   Yes, have added concerned content.

4. When mentioning the spectrum of ocean waves, such as JONSWAP one, please cite related references, e.g., [4, 5].

   Yes, have done.

5. Please add explanation about the procedure of your spectrum estimation in your model test, e.g., record length of measuring data, how to do the spectrum estimation in your model testing. Otherwise, the quality of your spectrum estimation may be uncertain, resulting in the uncertain analysis in this research quite uncertain and questionable.

   Yes, related content has been added.

2. Editing part

6. Please rewrite the sentences in line 51-57.

51 Wave tank tests in this paper are conducted with three significant purposes. Firstly, for validation of
52 dynamic response and the applicability of the novel experimental PTO simulation platform in a
53 certain continuous period of time in the case of a physical scaled WEC; secondly, with the application
54 of the experimental PTO, to investigate the output power efficiency and hydrodynamic response of
55 the WEC in both regular waves and irregular waves with different PTO damping strategies. Thirdly,
56 to find the best PTO damping coefficient under certain wave conditions, which might be seen as an
57 example use of the generic PTO simulation platform. Therefore, to indicate the potential use of the

Yes， have done.

7. In line 75, please replace Fang He by Fang.

   In line 77, please replace Fang he with Fang.

   Yes， have done.

8. In 84 Before the propose of the experimental PTO simulation platform, in[19] Saishuai Dai assessed the ,

please replace Saushuai Dai by Saushuai.

Yes, have done.

9. In 108 $m\ddot{x}(t)+c\dot{x}(t)+kx(t)=F_0\sin wt$ and 117 $x(t)=\frac{X}{2}\sin(wt-\frac{\pi}{2}+\beta)$, please replace "w" by "ω".

Yes, have done.

10. In 131 During Tank Testing, replace "Tank Testing" with "tank testing".

Yes, have done.

11. In line 128, please replace "Where" by "where".

Yes, have done.

12. The size is too small for Figs. 4-12, Fig. 14, Figs. 16 and 17. Difficult to read.

Yes, have improved each picture to a much better level.

13. The reference section may be enhanced by adding the following [1, 2] for wave spectra and [3, 4] for oscillations.

Yes, have done

[1] C. M. Harris, *Shock and Vibration Handbook*, 5th Ed., McGraw-Hill, 2002.

[2] M. Li, Three classes of fractional oscillators, *Symmetry*, 10(2) 2018 (91 pp).

[3] M. Li, Fractal time series — a tutorial review, *Mathematical Problems in Engineering*, vol. 2010, Article ID 157264, 26 pages, 2010.

[4] "The specialist committee on waves, final report and recommendations to the 23rd ITTC," in Proc. 23rd ITTC, 2002, vol. II.

[5] M. Li, A method for requiring block size for spectrum measurement of ocean surface waves, *IEEE Trans. Instrumentation and Measurement*, 55(6) 2006, 2207-2215.

Hydrodynamic responses and power efficiency analyses of an oscillating wave surge converter under different simulated PTO strategies

Xue Jiang [1], Sandy Day[1], David Clelland[1]

[1]: Dept. of Naval Architecture, Ocean and Marine Engineering, University of Strathclyde, Henry Dyer Building, Glasgow, G4 0LZ, UK

Abstract: Experimental investigation on the power performance of a bottom hinged oscillating wave surge converters (OWSC) with different power take-off (PTO) damping strategies (provided by a generic PTO simulation platform) are conducted in regular and irregular waves. The hydrodynamic performance of the OWSC under different damping modes, in regular waves and irregular waves, is observed. For regular waves, the effects of the main influential parameters (including the incident wave height, wave frequency, phase difference between the buoy velocity and wave elevation) on the output power were quantitatively studied. Six damping coefficients of the linear PTO damping is examined under constant incident wave height, and increasing wave frequencies and an output power curve along wave frequency are presented for each input gain of the PTO simulation platform in both linear damping mode and nonlinear damping mode. Additionally, the best coefficient or input gain is obtained for both linear or nonlinear PTO damping mode in different wave conditions. The phase difference between the buoy velocity and wave elevation of the OWSC model in irregular waves has the same trend as that in regular waves. The output electricity in the JONSWAP spectrum is found to be (approximately 300%) higher than that in a user-defined spectrum for the same wave parameters. However, nonlinear PTO strategies have no distinct advantage in the amount of electricity output but have better stability and broader damping range.

Keywords: Model testing, Oscillating type wave converter, Hydrodynamic responses, Output power curves, Different PTO strategies

Highlights:

- A series of output power curves are obtained, based on experiments for different PTO strategies on an OWSC model device.
- The power efficiency curves of an OWSC model in the JONSWAP spectrum under different water parameters are drawn.
- The best PTO damping strategy and the corresponding input gains have been achieved and attached.

Introduction

Marine energy conversion has been a concern for years. However, tests aiming at evaluating the global response of the system without properly considerating PTO systems can't predict the performance of a physical WEC device[1-5]. That might lead to errors in estimating the behaviour and efficiency of the full-scale device and negative profits for wave energy companies. PTO behaviour may be one reason why devices don't perform as well as might be expected.

Though the waves carry enormous power potential in the open sea which is claimed to be comparable to the world's current power consumption [6-10], the wave energy conversion technology only will be possible to meet the daily use of electricity cost-effectively. To enhance the cost-effectiveness, Fang et al. investigated the range of electricity-producing wave frequency by experimental study with asymmetric pneumatic chambers in [11], and the vortex-induced energy loss for OWC-Type breakwaters in [12]. Fang et al. also studied the characteristics of using orifices to model nonlinear power-take-off for an oscillating water column device in wave-flume tests[13]. There have been some literature reviews on PTO system, power performance and construction technology of WECs[14-21] , however there is no way to compare the efficiency of different PTO systems considering the vast difference existing among PTO mechanisms. The novel generic PTO simulation platform proposed in the companied paper makes it possible to compare the efficiency of the PTO damping with different coefficients, linear or nonlinear.

Before the propose of the experimental PTO simulation platform, in[22]Saishuai assessed the performance of a Fixed Symmetry Cylindrical oscillating water column (FSCOWC) device using orifice plates to represent the PTO system. And the comparison of numerical calculation and experiments proved that the scaling of the PTO for the tank testing is not a success. And in [23]Zhipeng et al. conducted a series of model tests for a heaving buoy wave energy converter in a wave flume, using various air dampers to simulate the PTO damping. There has no literature reporting about the tank tests with the consideration of a nonlinear PTO damping strategy, however, the nonlinear damping effects on WECs are significant as reported in some numerical study.

The oscillating wave surge converter (OWSC) is a kind of wave power generation technology, which makes use of the enhanced horizontal fluid particle movement of the waves in coastal areas, with a water depth of 10-20 meters. The OWSC mainly oscillates horizontally in the swell, rather than most wave devices, which swing vertically as they rise, and are usually deployed in the deeper water. And a simplified, scaled Oyster model is adopted in this study, because of the practical experience gained from Oyster1 and Oyster2. There were a few studies on the deployment, characteristics and hydrodynamic performance of Oyster model [24-27], while the published experimental studies were rare. There were still few efforts on the effect of PTO damping on the behaviour and power performance of a WEC. Furthermore, the power performance under different PTO strategies (linear or nonlinear, different damping coefficients) and the hydrodynamic effects from different PTO on the WEC have not been quantitatively investigated.

Therefore the authors focused on improving the power production of wave energy conversion by maximising the efficiency of the power-take-off system of wave energy converters (WECs). For this purpose, a PTO simulation platform proposed in the previous paper[28] of authors is adapted to produce a variety of different real-time damping force accordingly to different PTO strategies. Based on the prior study of simulating and quantifying of the PTO damping, the authors want to have an insight on the effect it has on the performance of a specific WEC, since the starting point of the study is that PTO behaviour may be one reason why devices do not perform as well as might be expected. Therefore, this paper concerns at the hydrodynamic response and power efficiency analyses of a bottom hinged oscillating type wave converter model (which is a 40^{th} scaled Oyster device) in regular and irregular tank tests under both linear and nonlinear PTO damping strategies.

Wave tank tests in this paper are conducted with three significant purposes. Firstly, to further validate the innovative simulation platform proposed in[28], by applying an OWSC device to the platform. Secondly, with the simulated real-time damping force(linear or nonlinear, various scaled)

used on the innovative simulation platform proposed in[28], to study the output power efficiency and hydrodynamic response of the OWSC in regular waves or irregular waves. Thirdly, to find the best coefficient of PTO damping force under different wave conditions, to indicate the potential use of the platform in giving a prediction for PTO optimisation. Take the OWSC in this paper as an example, best PTO damping coefficients are drawn for both linear and nonlinear damping for a certain scaled wave conditions, then the function of the best damping could be used to design a physical PTO system or value the potential to optimise an existing PTO system in the corresponding wave conditions.

In summary, a series of model tests are conducted in a wave tank to investigate the power performance of an oscillating buoy wave energy converter in regular and irregular waves under various simulated PTO damping strategies, with the idea to locate the best damping coefficient in mind. The effects of the incident wave amplitude, frequency and PTO damping on the dynamic response and power capture efficiency of the WEC are studied. The output power efficiency in irregular waves is also determined and compared with that in regular waves. Finally, conclusions are drawn from the study.

Experimental methodology

In developing a WEC, the critical issues are the assessment of the hydrodynamics. The responses of OWSC buoy involve complex interactions between waves and the structure with damping[29]. It is noted that only the pitch motion of the float is considered in this study, based on the operation principle of the OWSC. The governing equation of the buoy motion in surge can be expressed as below:

$$m\ddot{x}(t)+c\dot{x}(t)+kx(t)=F_0\sin\omega t \qquad \textit{Equation 1}$$

in which $x(t)$ is the instantaneous surge position of the buoy, $\ddot{x}(t)$ and $\dot{x}(t)$ are the acceleration and velocity of the float, respectively. m is the total mass of the system, which includes the net mass of the float m_0 and the added mass due to the fluid. c is the damping coefficient of the system, which includes the structural damping coefficient due to the mechanical friction c_0 and the external damping coefficient from the PTO c_p. k is the hydrostatic restoring force. ω is the angular frequency of incident waves, $\omega = 2\pi/T$, where T is the wave period. F_0 is the peak value of the wave excitation force. For the complete response to a system driven by $F_0\sin\omega t$, refer to[30-32].

The steady-state solution for Eq. (1) can be expressed as:

$$x(t)=\frac{X}{2}\sin(\omega t-\frac{\pi}{2}+\beta) \qquad \textit{Equation 2}$$

where X is the maximum surge displacement of the buoy, Initially, β should be the phase difference between the surge velocity and wave excitation forces, as the resonance is usually indicated by a zero value of β. For the present cases, the wavelengths are relatively more substantial than the geometry size of the buoy (L/D > 3.0, L being the wavelength and D being the geometry size of buoy, i.e., the width of buoy), which means the wave periods are sufficiently long in this study. It can be assumed that the wave excitation force is in phase with the wave elevation, as is asymptotically true for long wave periods[33]. Thus, in the following discussions, β is approximated by the phase difference between the buoy velocity and the wave elevation.

The absorbed power in this paper is defined as follows:

$$P = F_{damping} \times v_{WEC} \qquad \text{Equation 3}$$

where $F_{damping}$ is the damping torque applied on the wave converter, while v_{WEC} is the surging velocity of the converter.

And root-mean-squared power values are used to plot the power curves.

Model testing

During Tank testing, both regular wave tests and irregular wave tests are carried out. The tank tests of the PTO simulation platform in the case of a scaled bottom hinged. Oscillating wave converter (OWSC) is carried out at the smaller hydrodynamic lad in Henry Dyer Building of University of Strathclyde, which is 21.6m long, 1.6 wide and 0.45m deep.

3.1 Tank and model

Tank facilities: the experiment was carried out at the smaller Hydrodynamics Tank (Fig.1) of the University of Strathclyde. The tank is equipped with a highly repeatable four-flap type absorbing wave maker which consumes the reflected, radiated wave from the device and makes sure the generated wave is consistent during a single test. A high-quality variable slope beach is installed at the end of the tank to absorb equipped with a wall-mounted heater to minimise the temperature variation. Data acquisition is achieved by the PC based modular data acquisition system.

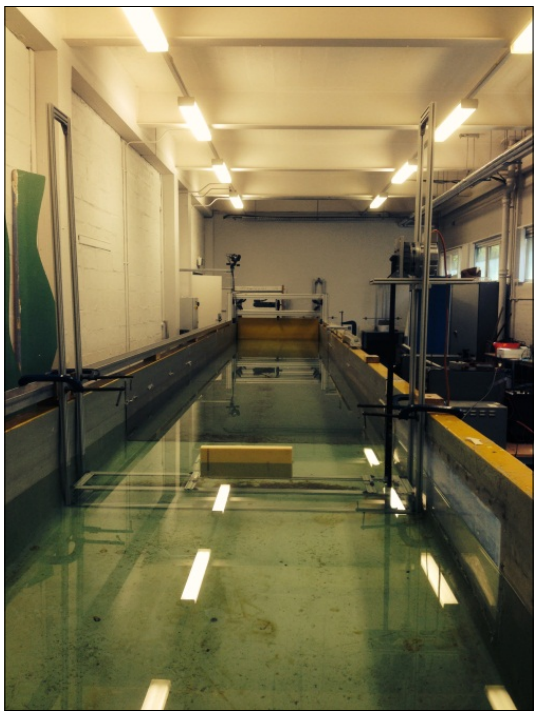

Figure 1 Hydrodynamic tank in Henry Dyer Building

Model：ITTC (International Towing Tank Conference) recommend that the ratio of the breadth of the device to the width of the tank should not exceed 0.25, to reduce the blockage effect caused by waves radiating off the tank walls. A scale of 40 is therefore used to size the paddle to as dictated by the breadth of the tank where the tests are conducted. The aspect ratio is kept relatively similar to the Oyster 800. Therefore, the geometric model scale ratio is λ = 1:40 and the scaling factors were determined according to Froude's law of similarity as shown in Table1, the modal is installed on an experimental frame as the paddle shown in Fig.2.

Table 1 General properties about the model

Full-scale parameters		Model parameters	
Paddle height	12.2m	***Paddle height***	305mm
Distance to seabed	16m	***Distance to bottom of the tank***	400mm

Experimental setup: as shown in Fig.2, on the frame stand which is consists of aluminium alloy profiles, one DC motor, two gears (one small, one big), two bearings, a rotary axel and a 1/40 scaled model paddle are installed on it. The paddle is the surging buoy that has a large surface area and is easily excited by waves. The paddle is attached to a rigid aluminium alloy plate, which in turn connects to a stainless steel axel. The paddle, plate and axle act as a rigid body. The stainless steel axle runs through two bearings. This allows the paddle to pitch smoothly, and the simulated PTO damping to be applied to it. The bearings are attached to a stationary rigid aluminium alloy frame, and the rotation of axel caused by the surging paddle is transferred to the other shaft of a gear–belt-gear system, enable the motor to stay out of the water, at the top of the frame. Thus the wave force can be transferred to the output shaft of the motor, where a damping torque following the programming in myRio controller is produced while electricity is drawn from wave motions.

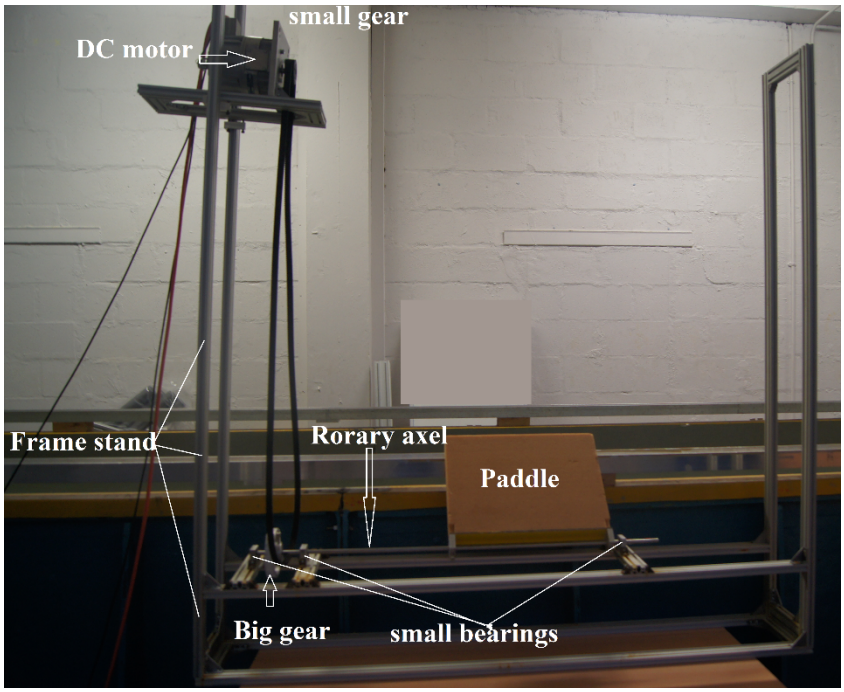

Figure 2 Experimental setup

Transfer mechanism: to successfully transfer the motion of paddle to the output shaft of the motor, a pre-tension is applied on the belt, and the belt tension mainly depends on the height of the stand, as shown in Fig.3. So for designing the frame stand, we take both the most considerable wave heights and the nearest standard timing belt into consideration, aiming at finding a height enough higher than the highest wave and slightly higher than a specified standard timing belt. Besides, the belt is made from neoprene, which is a corrosion resistant material and slightly extends under fatigue since it is critical to guarantee the excellent quality transmission of the motion of the paddle. The transfer ratio produced by the timing belt is 9.6.

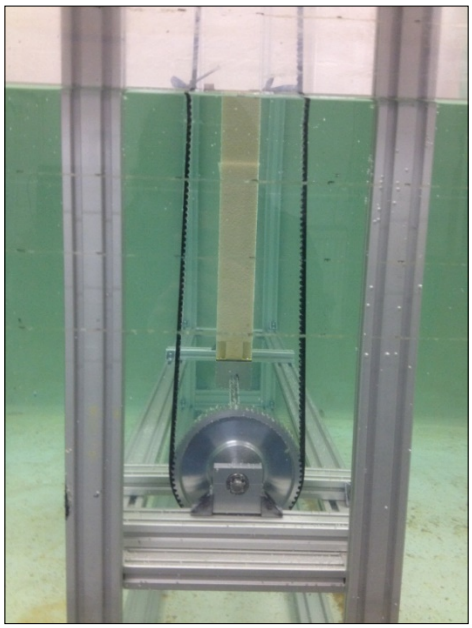

Figure 3 Photo of belt tension

Calibration of wave probes: the water surface profile was measured via two-wire resistance type wave probes. The model was set at 9m downstream of the wave generator, and two wave probes are placed to measure the wave elevation as shown in Fig.4. Before installation, the probes are calibrated by moving up and down on a calibration frame with holes precisely machined at 5mm intervals. The wave probes were calculated over a range of +/-40mm, with the main focus on waves of +/-20mm. A calibration curve is given below in Fig.5. As the typical linear fitting curve and the fitted conversion equation show, the conversion coefficient for the inlet wave probe above zero is 92 with a bias as 0.24mm. And similarly, it is obtained the conversion coefficient 94 for inlet wave probe below zero with a bias as 0.39. For Fixed wave probe, it is 97 with a bias 0.26mm above zero and 96 with a bias as 0.8 below zero.

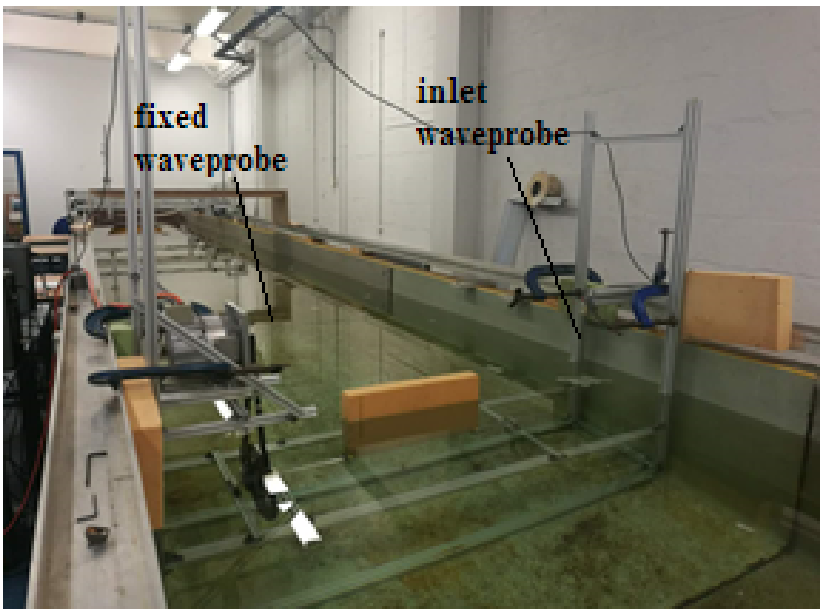

Figure 4 Experimental Setup

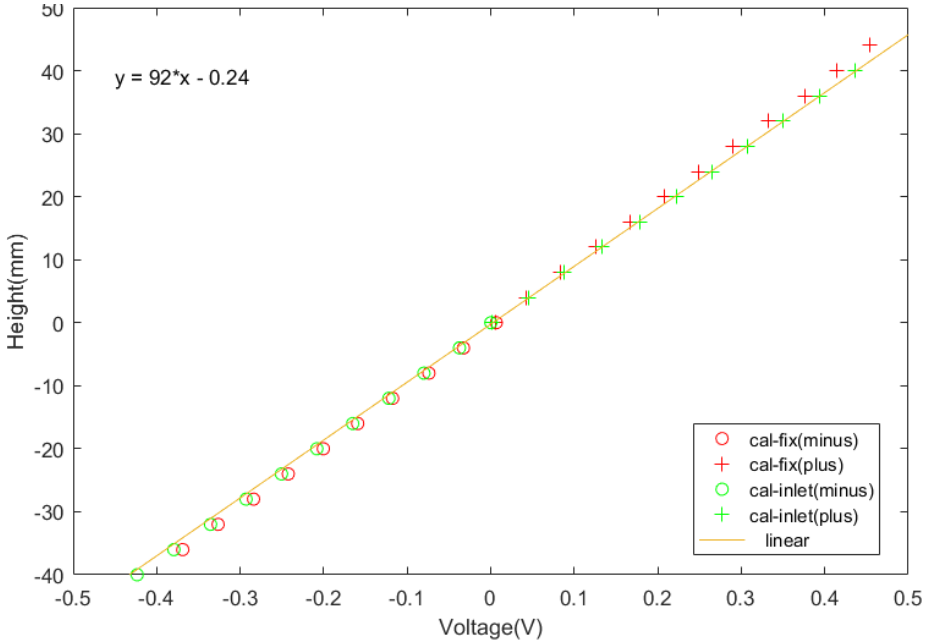

Figure 5 Calibration of wave probes

Data monitor: similarly as in the previous paper demonstrating the calibration of the PTO force simulation platform[28], monitor torque, position and velocity are measured voltage from the tachometer, current from the current sensor, which is time-continuously monitored by a DAQ system, to give a prediction of the rotating speed, damping torque and the paddle position.

3.2 Regular wave tests

3.2.1 Test matrix and data process for regular waves

A 1/40 scaled model of Oyster is adopted, and the scaled water parameters are obtained according to Froude's law of similarity, and they are listed in Table 2.

Table 2 Parameters used in regular wave tests

Full scale		Tank scale	
Wave Height	2m	***Wave Height***	50mm
Water depth	25.2m	***Water depth***	630mm
Wave frequency	0.06-0.2372Hz	***Wave frequency***	0.4-1.5Hz

For one PTO damping simulation, 12 wave frequencies were used for 12 experiments in the regular wave experiment. And seven linear PTO damping simulations and seven nonlinear PTO damping simulations are used to collect data for the purpose of observing the behaviour of the output power. The gains are input parameters used in the control function of the software in the loop for producing PTO damping. As concluded in the companied paper, each gain can be regarded as a damping coefficient in either linear cases or nonlinear cases. The gains selected for use are listed in Table 3.

Table 3 Parameters used for different PTO strategies

Frequency(Hz)	0.4	0.5	0.6	0.7	0.8	0.9	1.0	1.1	1.2	1.3	1.4	1.5
Gains for linear damping	20	40	70	80	90	100	120					

Gains for nonlinear damping	20	40	80	120	160	180	200	

As shown in Table 3, if N_f is the number of frequencies (12), N_g is the number of gains (7*2), N_t is the number of tests, then the relationship is described as follow:

$$N_f \times N_g = N_t \qquad \textit{Equation 4}$$

And N_t should be 168, therefore for regular waves, 168 individual tests are carried out. And for each test, a typical data monitor and processing method is demonstrated as below.

3.2.2 The behaviour of output power

In this section, we have an insight on the impacts the linear PTO damping or nonlinear damping has on the output power. Take the test under linear damping of gain 80 and frequency 0.8Hz as an example. Data is first monitored at a sampling 100Hz, as shown in Fig.6 (a&b). It is learned from Fig.6(a) presents the time history of input velocity and output velocity, wave elevation measured from t that due to the existence of the simulated PTO damping the real-time output wave velocity is smaller in amplitude than the input wave velocity to the paddle, and the elevation measured by the inlet wave probe which is the wave elevation after push the paddle to produce electricity, similarly the elevation measured by the fixed wave probe placed long enough before the paddle is waves before experience the paddle. Moreover, the PTO damping force is measured as well which is shown in Fig.6(b).

（a）

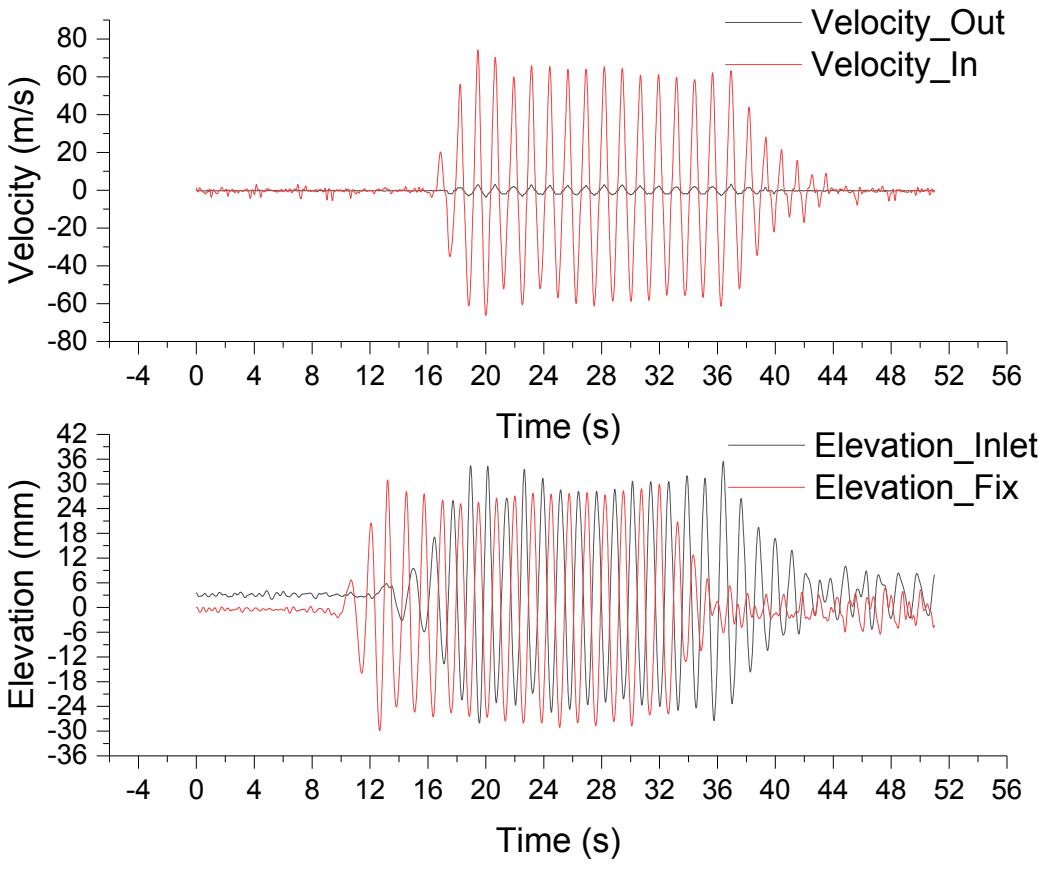

226

(b)

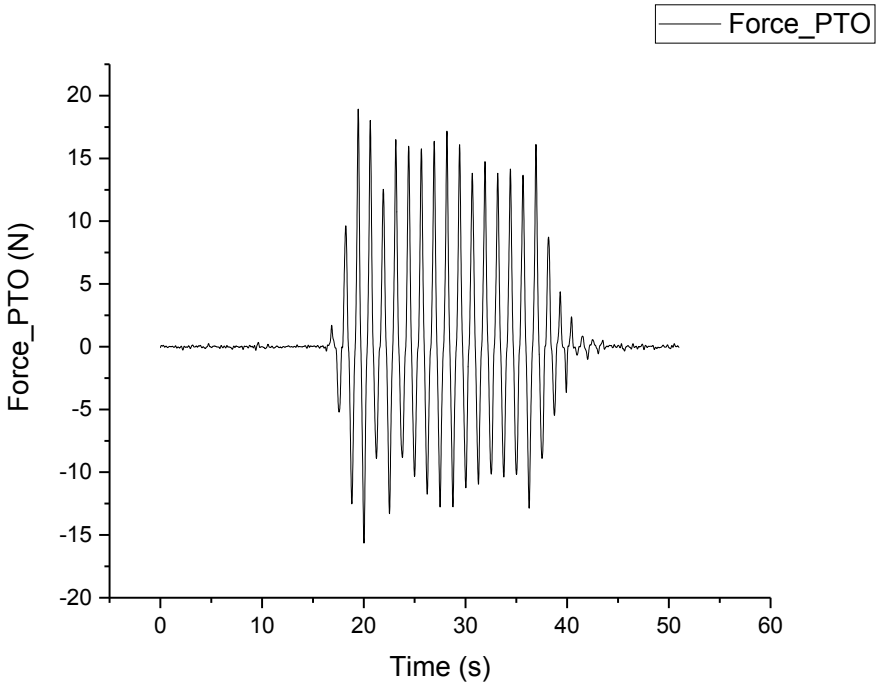

227

228 **Figure 6 Time history of the significant data monitored from one typical test**

229 Then the output power is obtained by equation1, as shown in Fig.7(b). Moreover, a few of the cycles
230 of the signal are selected for the root-mean-squared (RMS)calculation of the power as shown in
231 Fig.7(a), and the RMS value is used as a predicted power output when the PTO strategy is linear
232 damping under gain80, and when the wave height is 4m, the wave frequency is 0.8HZ.

233

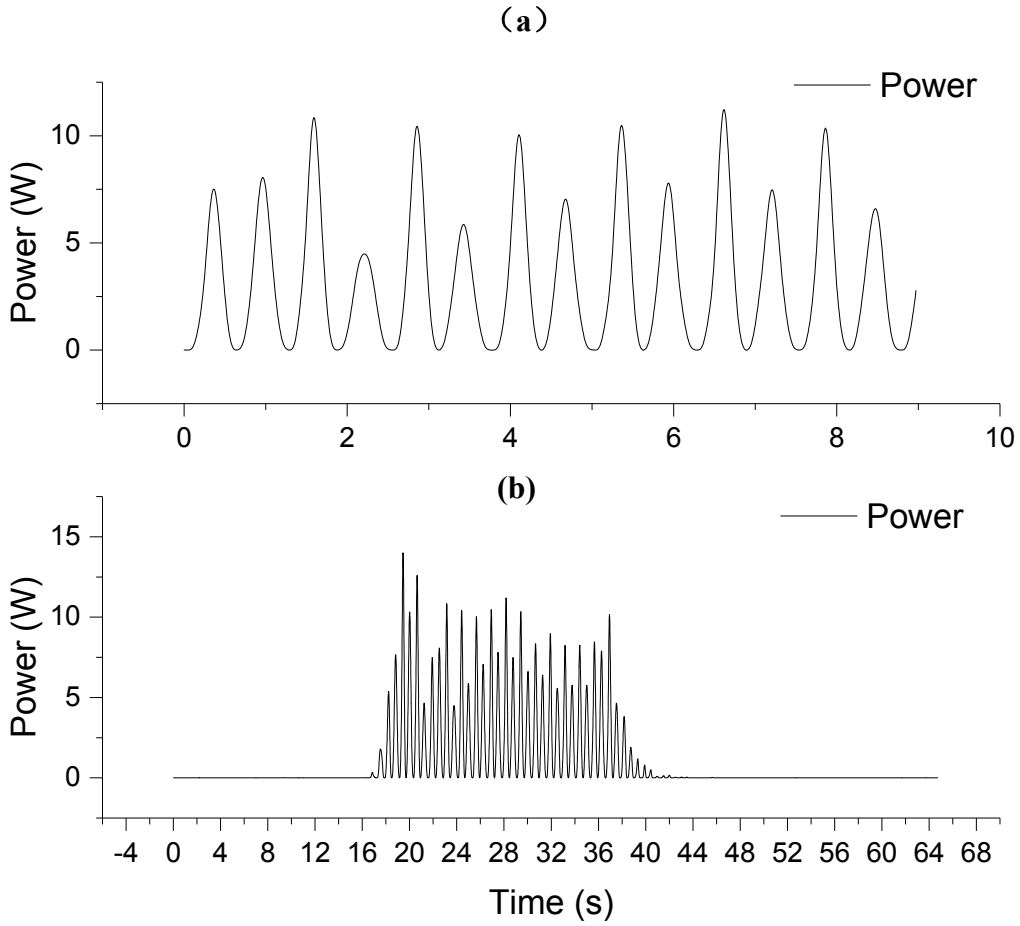

Figure 7 Time history of output power :a) the selected data from (b) used for statistical analysis; b) the output power for one typical test

The root-mean-square power values are used to plot the coherence between the absorbed energy and the wave frequency as shown in Fig.8 and Fig.9. From Fig.8 we can generally conclude that the linear damping with gain 80 (the corresponding damping coefficient is 139 in CCW rotation and 133.4 in CW rotation, see in the companied paper, section 4.3.1) is the best linear PTO damping, with which the OWSC absorbs the maximum power from the wave movement.

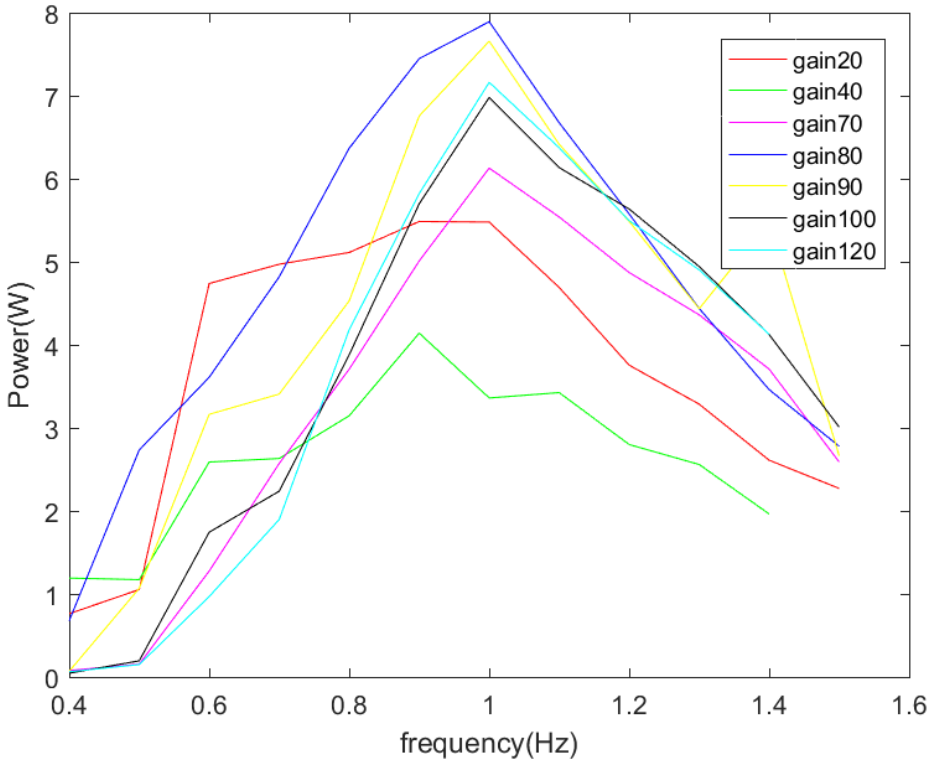

Figure 8 Power output curves for linear damping

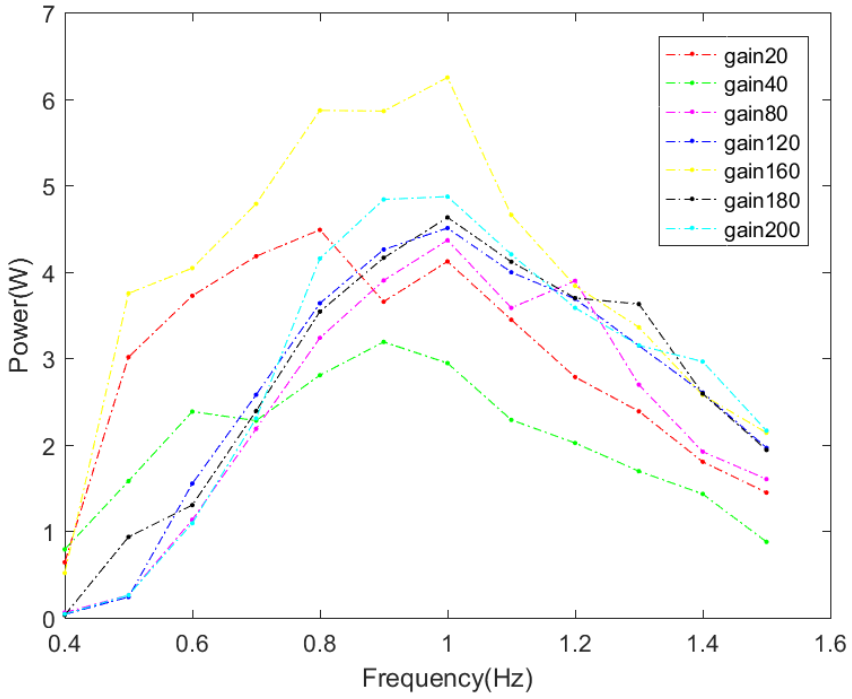

Figure 9 Power output curves for nonlinear damping

Similarly, as shown in Fig.9, we learn that the quadratic PTO damping works best with the input gain of 160 (the corresponding damping coefficient is 51.93 in CCW rotation and 53.21 in CW rotation, see the paper[28], section 4.3.2). For nonlinear damping, the lowest damping coefficient (gain20) copes

well with the ocean waves in low frequency. For higher frequencies (above 0.9Hz) the output power generally increase while the damping coefficient increase in between gain 40 and gain 160, it reaches the maximum at gain160, and starts decrease while the coefficient increase. For linear damping, the lowest damping coefficient also (gain20) copes better than gain40 and gain70, shows its advantage in low-frequency waves. And the output electricity is shown to increase as the linear damping coefficient increase and reach a maximum at gain80, then starts to decrease as the gain increase.

It is noticeable that the curves are not as smooth as expected, and the authors believe a few reasons which caused the fluctuation of the curves are displayed below:

1) The insufficient sensitivity of the wave probes, because the wave height measured by the wave probe is changing as the wave frequency varies, and the changing in the measured wave height is ignored during data process and plotting.
2) As discussed in the paper[28], there is a certain amount of uncertainty existing in the PTO simulator.
3) The Scaled OWSC device model is minimal to represent the real mass and real conditions of an actual OWSC device.

3.2.3 Hydrodynamic performance of the model

As discussed in [19, 34-36], the dynamic response may have a significant effect on the power performance of ocean wave energy converting devices. The resonance is usually indicated by a zero phase difference between the buoy velocity and wave excitation force. For the present study, this corresponds to a zero phase difference between the buoy velocity and wave elevation. Fig. 10 shows the time histories of the wave elevation ration $R(t)$ and buoy motion in pitch $x(t)$ for different damping coefficients under the wave frequency of 0.8Hz. It can be seen that there is no apparent difference observed for different damping coefficients, which means this phase difference is not PTO dependent in the case of a scaled Oyster model. Therefore, experiments base on the PTO strategy of linear_gain80 and nonlinear_gain160 are taken for examples to further study the behaviour of the phase difference. And the damping torque (which equals the excitation force) is observed in the phase of the rotating velocity of the paddle when wave frequency is above 1.0Hz as shown in Fig.11 and Fig.12. And the introduced ration $R(t)$ is defined by as below for the analyses of hydrodynamic performance in the following.

For wave elevation $R_a(t) = \dfrac{a(t)}{\max[a(t)]}$

For paddle velocity $R_v(t) = \dfrac{V(t)}{\max[V(t)]}$ *Equation 5*

In which $a(t)$ is the wave elevation, $\max[a(t)]$ is the maximum value of the wave elevation, $R(t)$ is the 'Ratio' as shown in Fig.10-12.

283

（a）

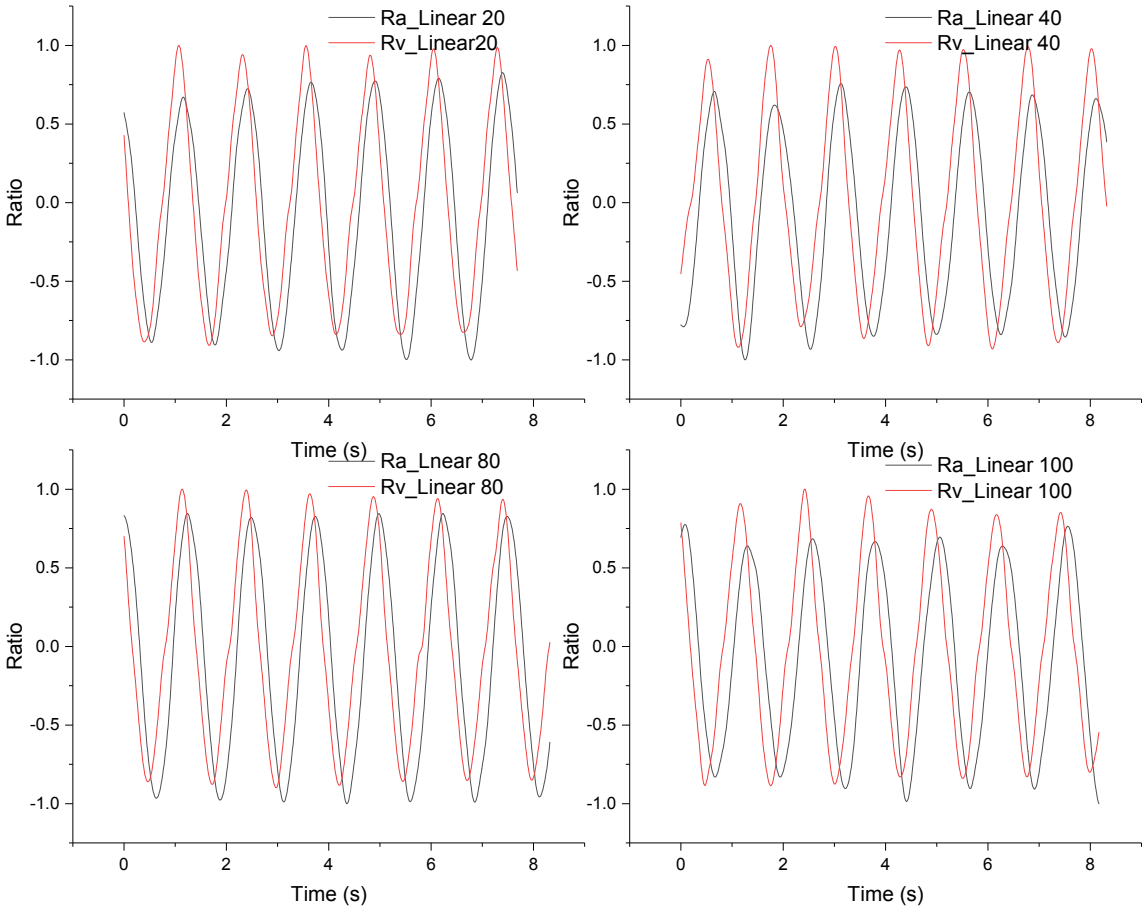
Ra_Linear 20
Rv_Linear20
Ra_Linear 40
Rv_Linear 40
Ra_Lnear 80
Rv_Linear 80
Ra_Linear 100
Rv_Linear 100
Ratio
Time (s)
1.0
0.5
0.0
-0.5
-1.0
0
2
4
6
8

284

(b)

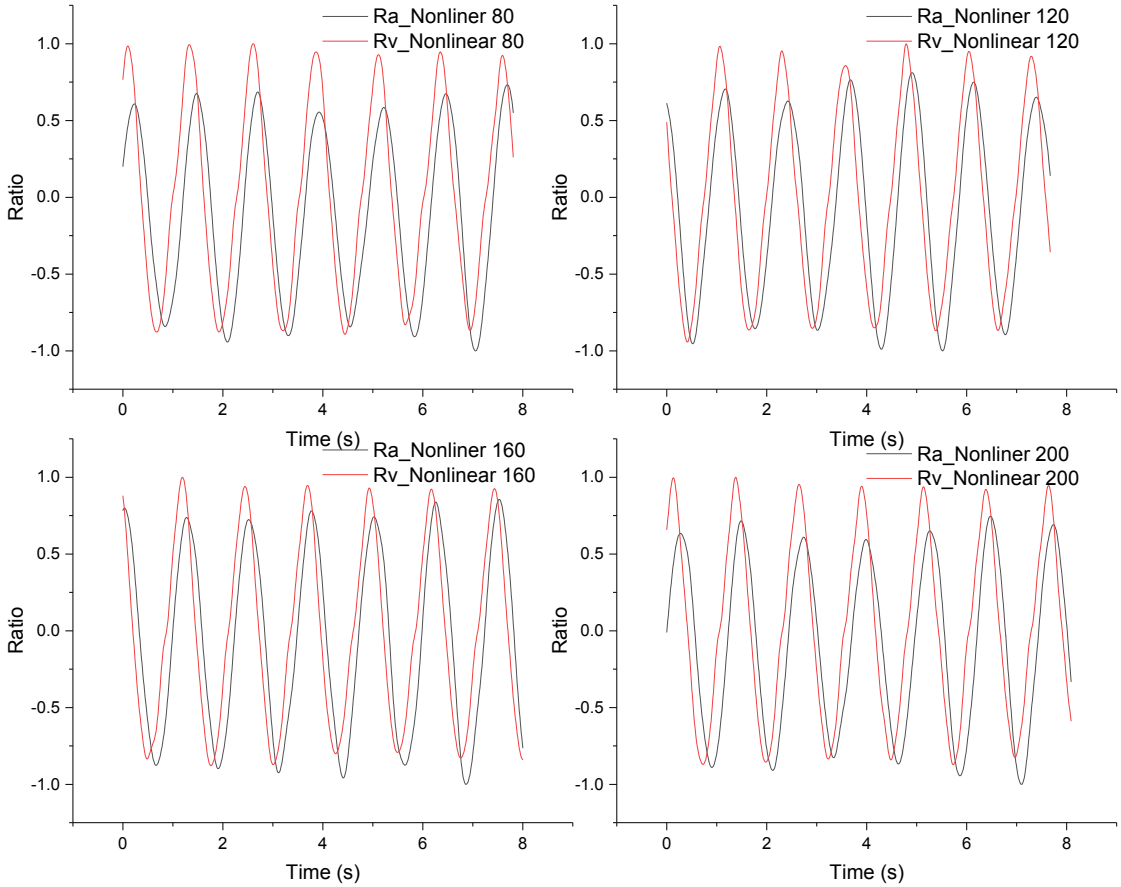

Figure 10 Time history of the ratio of wave elevation and buoy velocity for different input gains in regular wave tests under 0.8Hz; a) is for under linear damping, b) is for under nonlinear damping

Fig. 11 shows the time histories of the wave elevation ration $R(t)$ and buoy motion in pitch $x(t)$ for one standardized damping coefficient under different wave frequencies between 0.4Hz-1.5Hz. The instantaneous buoy velocity $\dot{x}(t)$, which is monitored by a tachometer concerning time t regarding the paddle velocity during the experiments, is also shown in the Figures. The time difference between the buoy velocity $\dot{x}(t)$ and wave elevation $a(t)$ is denoted as Δt, as shown in Fig. 11. Thus, the phase difference can be obtained by the relationship:

$$\frac{\beta}{2t} = \frac{\Delta t}{T} \qquad \textit{Equation 6}$$

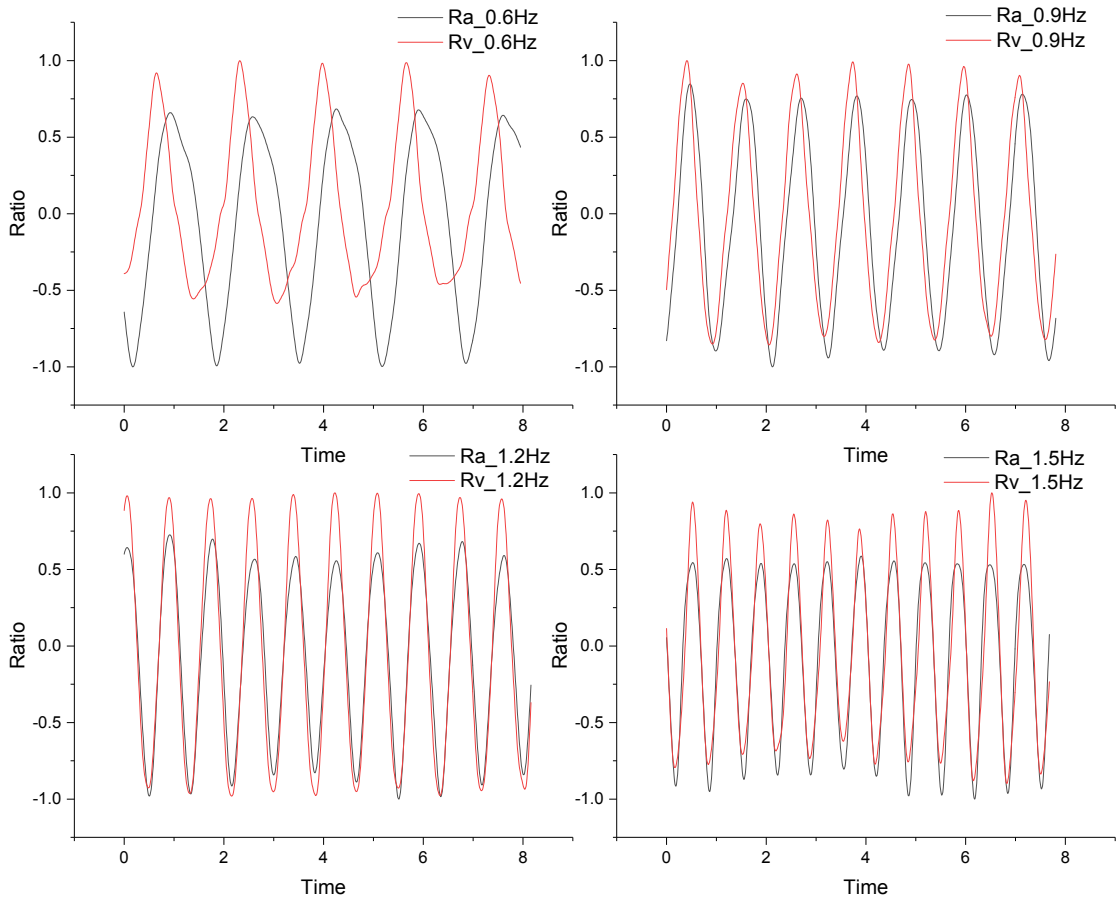

296

297 **Figure 11 Time history of the wave elevation and buoy velocity in regular wave tests under linear**
298 **damping of gain80**

299 It can be seen from Fig.11 and Fig.12 that the buoy moves with the same period as the incident waves,
300 but the phase difference between the buoy velocity and wave elevation decreases with an increase in
301 wave frequency, and resonance is indicated usually happen when the wave frequency is above 1.0Hz.

302 **(a)**

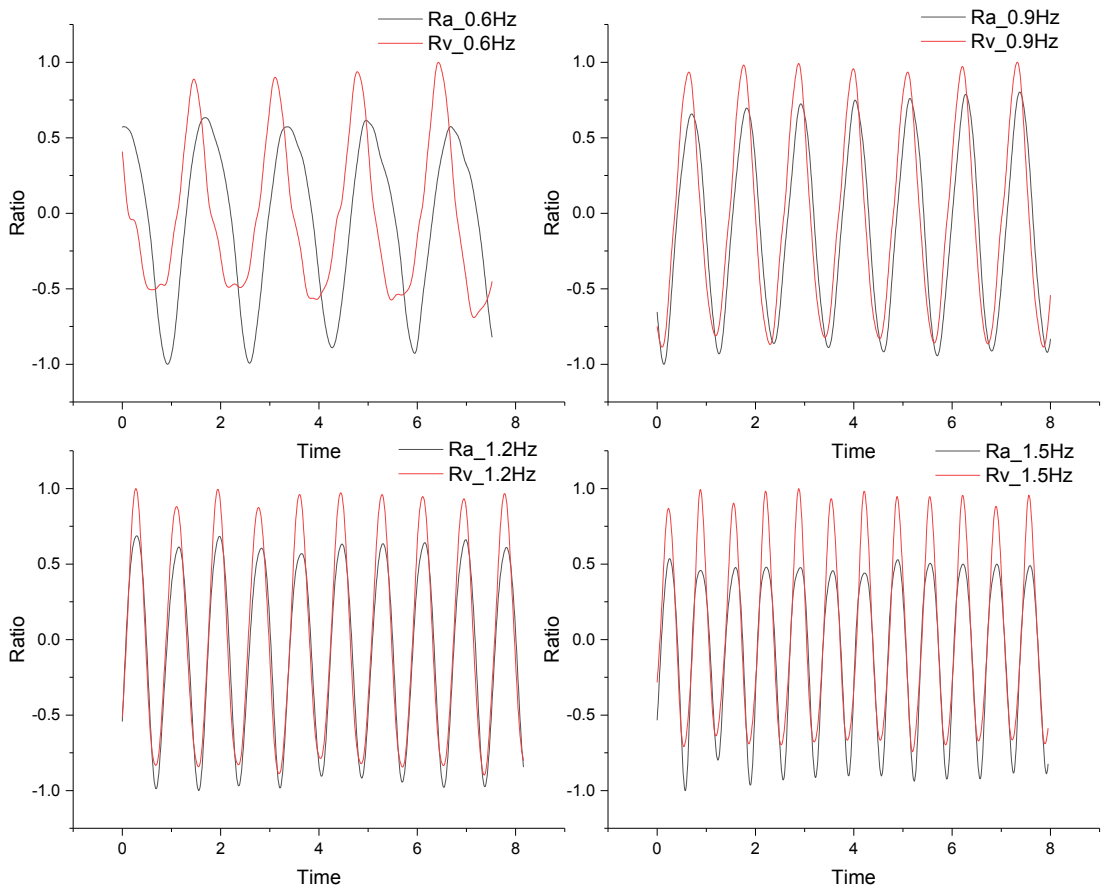

Figure 12 Time history of the wave elevation and buoy velocity in regular wave tests under nonlinear damping of gain160

3.3 Irregular wave tests

3.3.1 Test matrix for Irregular waves

Irregular sea states indicate wave conditions and energy distribution within the expected frequency range for given wind speed in the ocean or at a specific location in the sea. Some well-recognised spectra corresponding to particular areas can be applied to models in tank testing equipment. For the well-estimated JONSWAP spectrum. Therefore, during the irregular wave tests, both a user-defined wave spectrum and a generic JONSWAP spectrum[37, 38] are adopted The spectra are applied by computer software in the testing facility which directs the wave maker to produce the desired wave conditions. Data measuring of each tank test runs for 450s to reduce the transient response caused by the start and stop of the facility in the tank. However, the authors believe the testing results based on JONSWAP spectrum might have more academic meaning to publish, this section is mainly focused on the tests based on JONSWAP spectrum as shown in Fig.13., and the result of from tank tests under user-defined spectra are reviewed as a comparison in the following section.

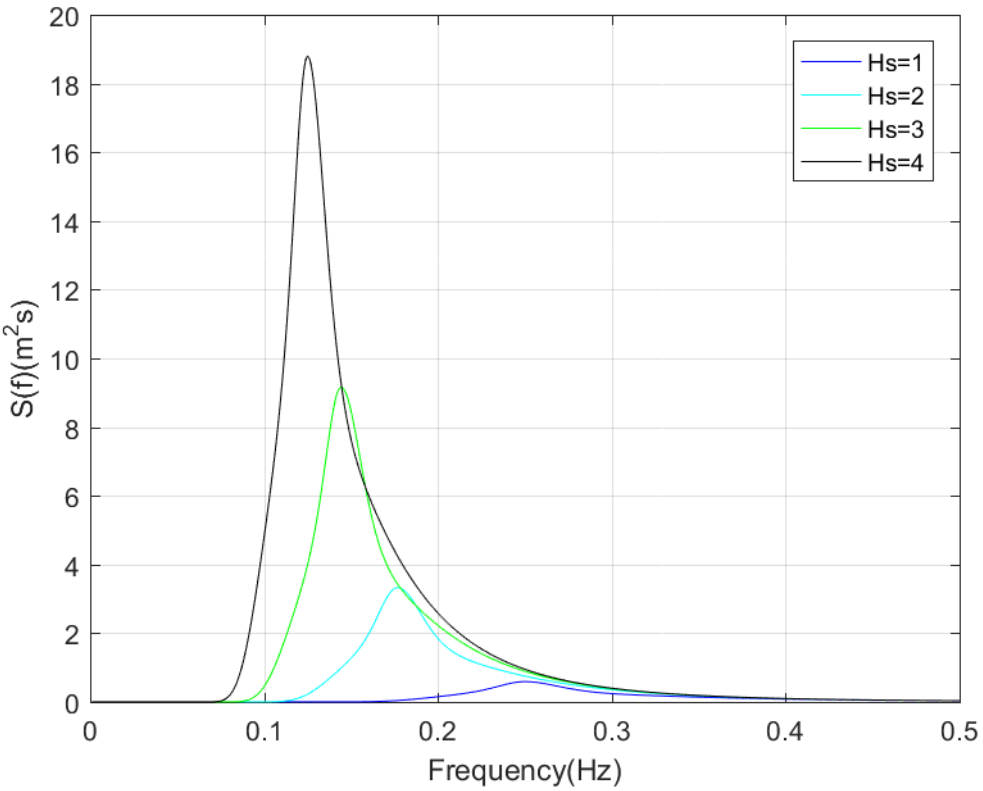

Figure 13 JONSWAP spectrum used in the irregular tank tests

It is noted by researchers [39-41] that there are two main parameters determine the shape of the JONSWAP spectrum and the specific sea conditions generated. They are mean wave period T_p and the significant wave height H_s. T_p and H_s are related by the following equation;

$$T_p = 4 \times \sqrt{H_s} \qquad \textit{Equation 7}$$

As mentioned in section 2.1, the model is a 40th of the existing device of the 'Oyster 800'. The duration of the test for the irregular spectrum is calculated according to the Froude's law of similarity,

$$T_{test} = \frac{T_{full}}{\sqrt{R}} = \frac{T_{full}}{\sqrt{40}} \qquad \textit{Equation 8}$$

Where T_{full} is usually 30 minutes.

The parameters used for the JONSWAP spectrum and tank tests are listed in Table 4.

Table 4 Spectrum parameters

Spectrum Parameters		Test parameter
Wave height(H_s)	4* $\sqrt{H_s}$ (T_p)	30m/ $\sqrt{40}$ (T_{test})
1m	4s	285s
2m	5.66s	285s
3m	6.93s	285s

4m	8s	285s

3.3.2 The behaviour of output power

Unfortunately, due to the limitation of the time of using the hydrodynamic tank, a limited number of irregular wave tests based on the JONSWAP spectrum as mentioned above are carried out, unlike in regular wave tests, 12 trials for each gain are carried out, whose file names in the supplementary data library is listed in the appendix. However, Table 5 lists all the file names (all files are supplied) obtained for irregular wave tests based on JONSWAP spectrum.

Table 5 Test files based on JONSWAP spectrum

Linear Damping							
H_s=1m	gain80	gain120					
Filename	h1l8r	h1l12r					
H_s=2m	gain80	gain90	gain120	gain400	gain800	gain0	gain-80
Filename	h2l8r	h2l9r	h2l12r	h2l41r	h2l83r	h2l0r	h2ln8r
H_s=3m	gain80	gain90	gain120	gain400	gain800	gain0	gain-80
Filename	h3l8r	h3l9r	h3l12r	h3l41r	h3l83r	h3l0r	h3ln8r
Nonlinear damping							
H_s=1m	gain160						
Filename	h1n16r						
H_s=2m	gain80	gain160	gain200	gain400	gain1200	gain2000	gain-160
Filename	h2n8r	h2n16r	h2n20r	h2n41r	h2n125r	h2n0r	h2nn16r
H_s=3m	gain80	gain160	gain200	gain1200	gain0		
Filename	h3n8r	h3n16r	h3n20r	h3n125r	h3n0r		

A MATLAB programme is written to calculate the data from each test file, and a few statistic values for relevant parameters are obtained, for instance, the standard derivation of wave height, the RMS of damping torque, the RMS of output power from the paddle calculated from equation1. And the RMS power values for each test files are used to draw the power curves against wave heights and PTO damping as shown in Fig.14. It can be seen from Fig14, the output power of the OWSC model(paddle) increase linearly as the wave heights increase, and the linear curve for bigger damping coefficient tends to have a bigger slope, though the power reaches the maximum at linear damping gain80 and nonlinear damping160 in regular wave tests. And it is seen from Fig.15, for the same significant wave height, the output power for linear damping is slightly higher than the nonlinear damping, though it may result in less stability in the corresponding PTO system.

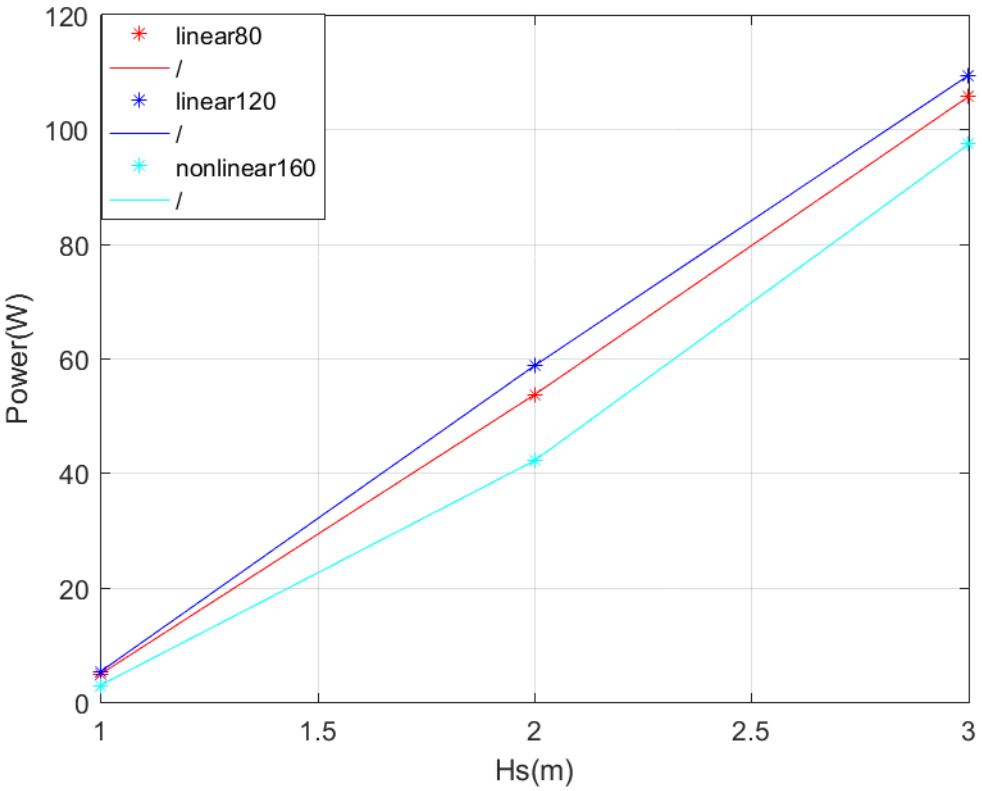

Figure 14 Power changes along wave heights

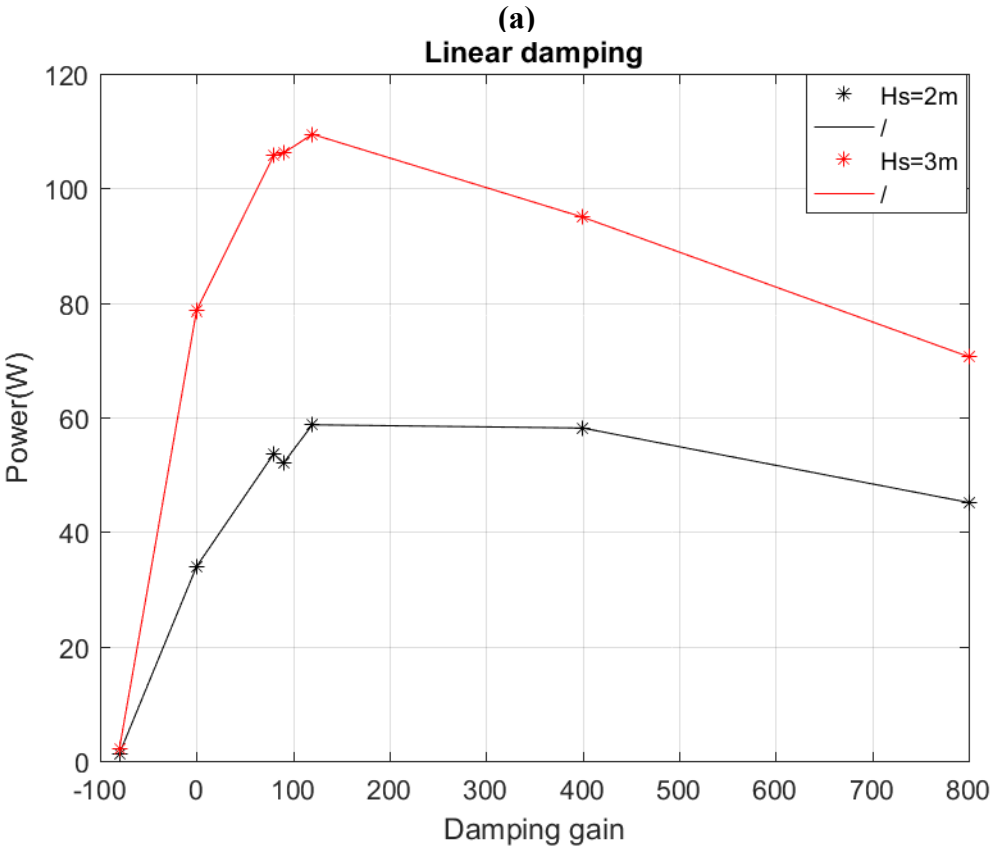

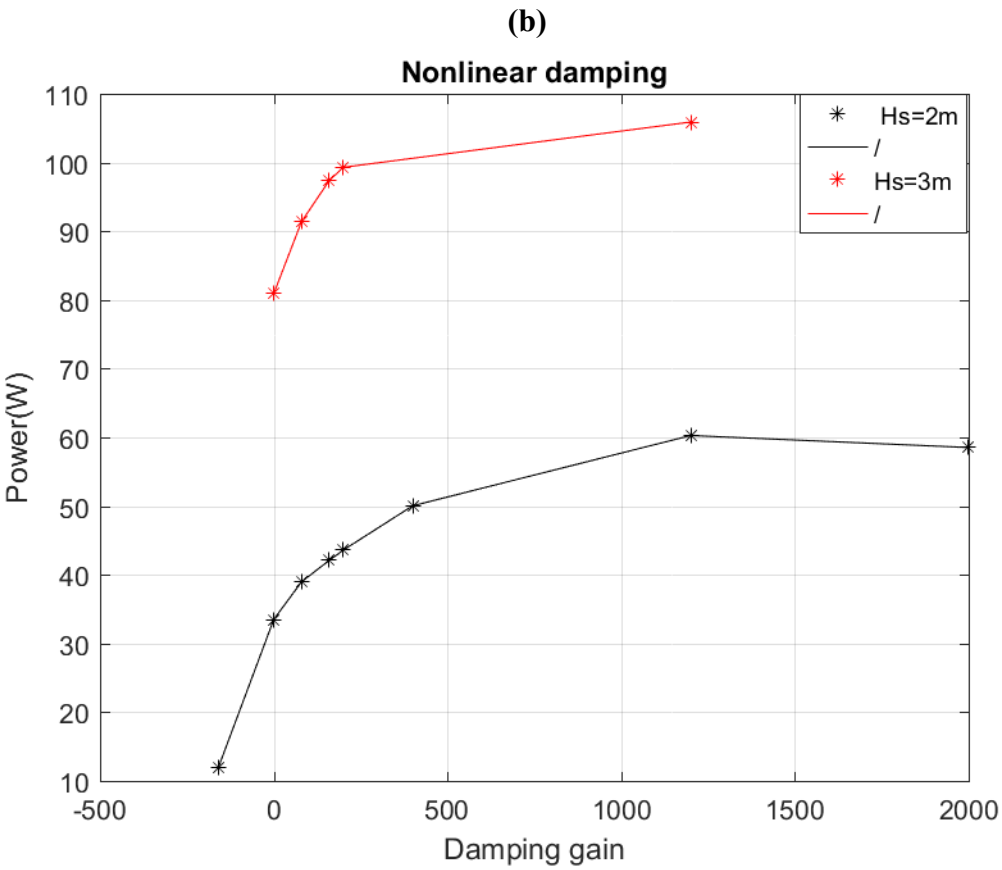

Figure 15 Power changes along input gains for linear PTO or non-linear PTO: a) is for linear PTO; b) is for nonlinear PTO

Fig.15 presents the changing of output power along with the changing of damping gains for two different significant wave heights, namely when Hs=2m and Hs=3m. The yellow one is for 3m, and the black one is for 2m. Each star point located on the line is an RMS value of the output power from each test file. As shown by the two lines, it is concluded the output power increase hugely as the PTO damping increase before it reached gain100, and it keeps almost stable in between gain100 and gain500, then reduce slightly when its further increase. Similarly, the power increase much less hugely than in linear damping cases, and tends to be stable when it reaches gain500, and it keeps almost stable even when the damping gain increase to 2000. Therefore, it is believed by the author that the nonlinear damping has a wider gain range and have better gain applicability though it does not show much advantage on the increase of power amount. Moreover, it is also proved for both linear damping and linear damping, that higher significant waves produce more electricity if without consider the stability and the robustness of the real PTO system.

3.3.3 Hydrodynamic performance of the model

During the irregular wave tests, a few overtopping is observed as shown in Fig.16. Overtopping is believed can significantly reduce the power output by[42, 43], when the wave passes over the top of the paddle, and it was therefore expected that the results might not be what was initially expected[44]. However, the output power curves indicate that it may not have a significant influence.

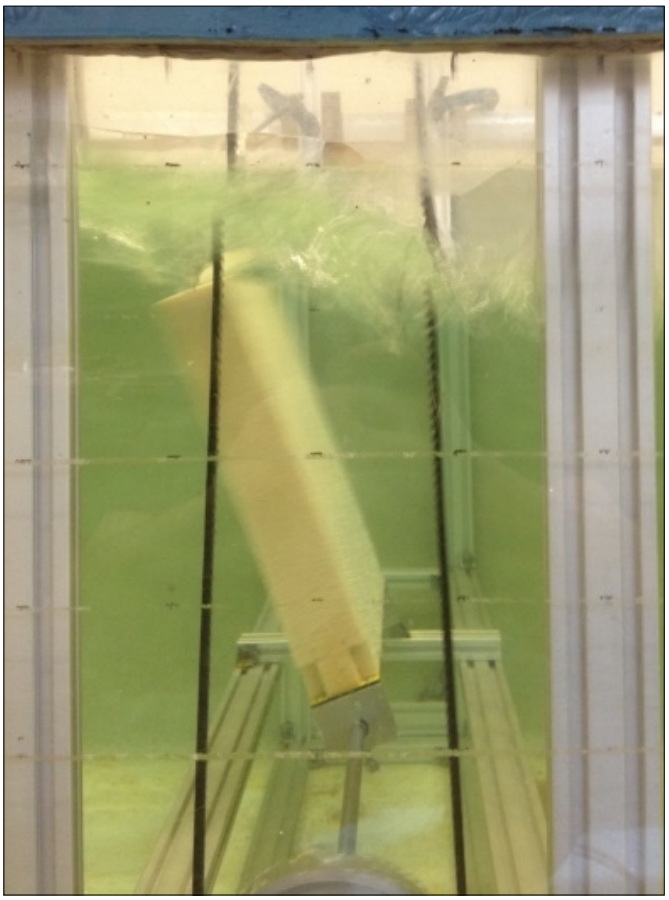

Figure 16 Side view of the effects of overtopping

As mentioned in section2.2.3, an amplitude ratio is defined during the observation of the hydrodynamic performance of the model in tank testing. And Fig. 17 shows the time histories of the wave elevation ration $R(t)$ and buoy motion in pitch $x(t)$ for the linear damping gain80 in random wave testing under JONSWAP spectrum when Hs=3m. Fig.18 presents the time histories of the wave elevation ration $R(t)$ and buoy motion in pitch $x(t)$ for the nonlinear damping gain160 during the same seconds and under the same wave spectrum. It can be seen from the pictures that there is no significant difference in the phase of whether adopting the linear PTO or nonlinear PTO strategy. And the paddle velocity is slightly behind but following the inline wave movement.

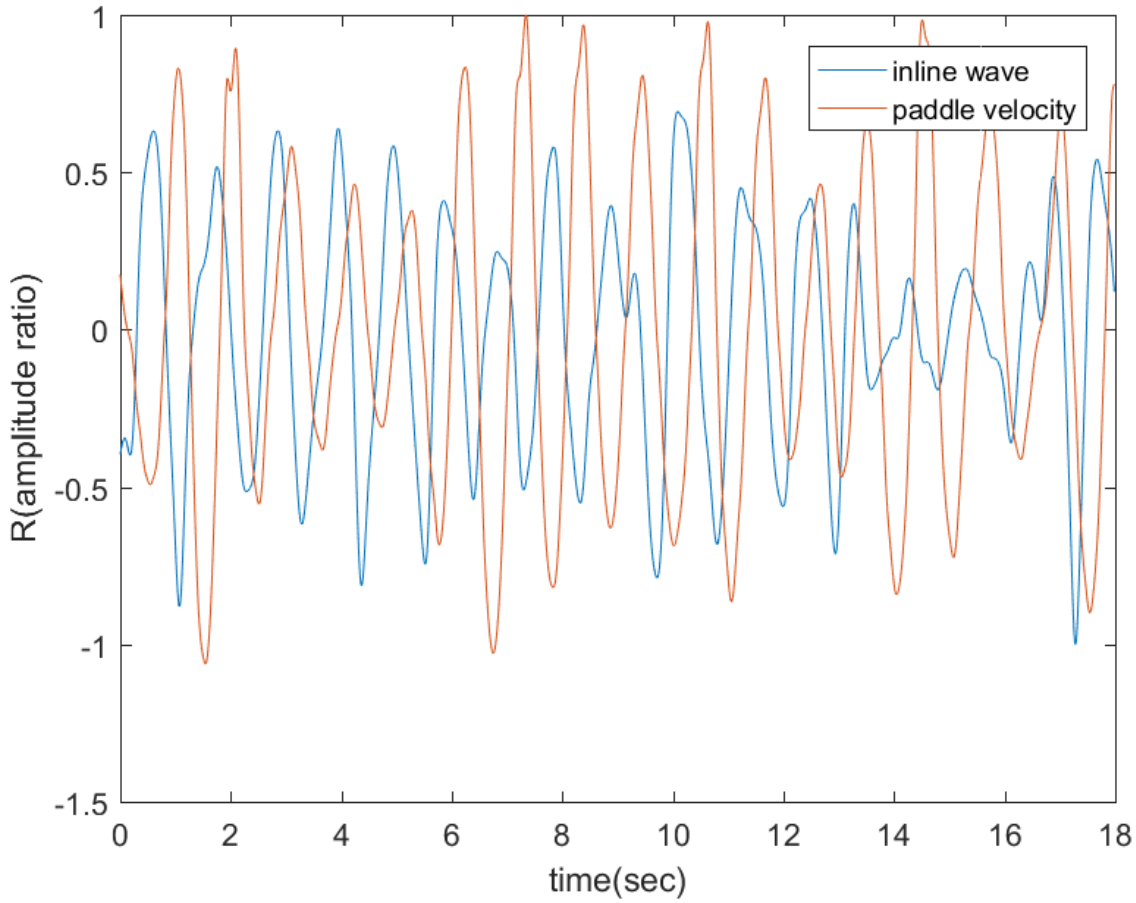

Figure 17 Time history of the wave elevation and buoy velocity in irregular wave tests under linear damping of gain80

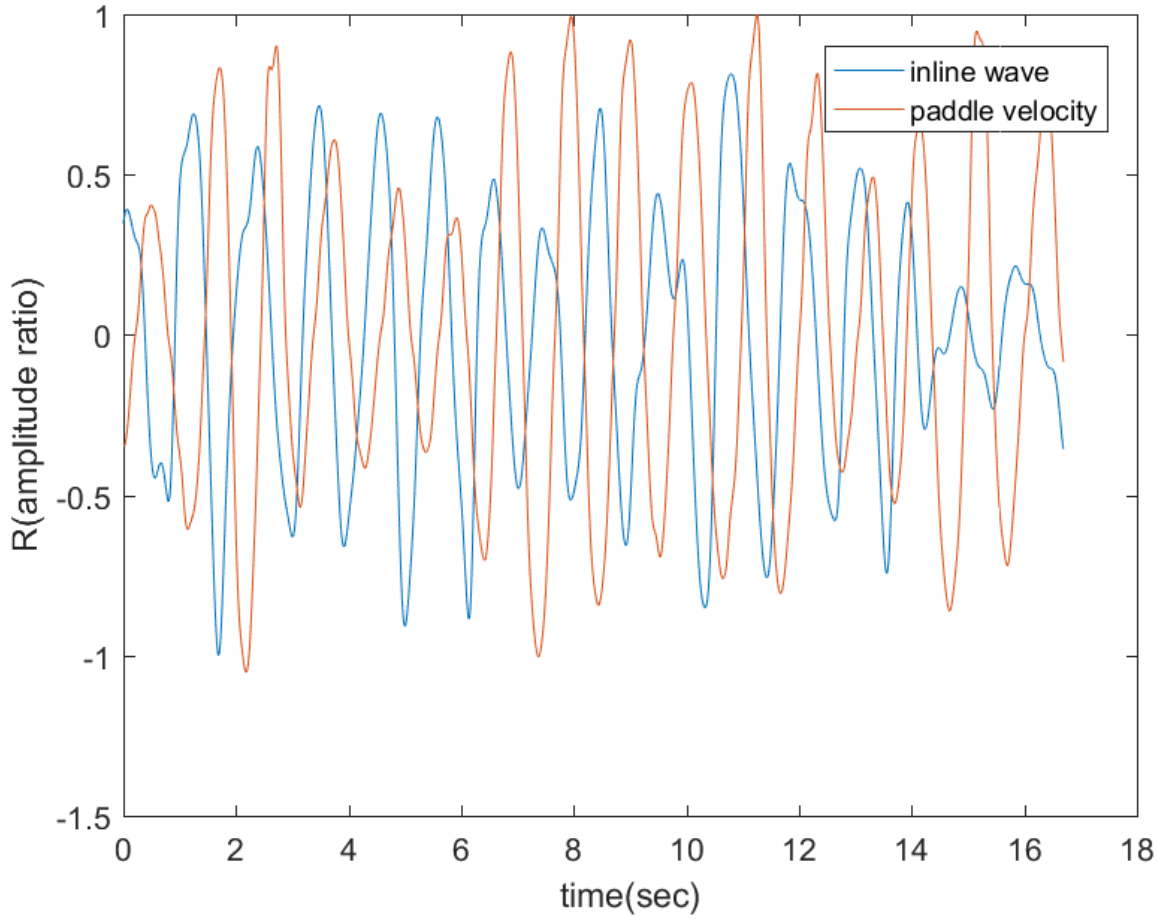

Figure 18 Time history of the wave elevation and buoy velocity in irregular wave tests under nonlinear damping of gain160

The final response is not pure sine so that it can be written as:

$$x(t) = \frac{X}{2}\sin(\omega t - \frac{\pi}{2} + \beta) + epsilon(t) \qquad \textit{Equation 9}$$

where $epsilon(t)$ is a non-sinusoidal component, whose energy is small, and the sinusoidal response is the principal component of the response.

The JONSWAP and the user-defined spectrum used in experiments are both unimodal, and the main energy is determined by the frequency at that peak. The response energy of other frequencies is small. Therefore, the sinusoidal response is roughly presented, also see in Fig.17 and Fig.18.

Comparison of the output power in regular wave and irregular wave

4.1 Comparison between linear damping and nonlinear damping in regular wave tests

Though the linear damping and nonlinear damping have best electricity output power at different gains, and the nonlinear damping has much wider gain range, it is critical to learning the different output behaviour at the same gains for linear PTO damping and nonlinear PTO damping. Therefore, Fig.19 shows the power comparison of the same gains for both linear damping and nonlinear damping.

It is seen that, for the same gain, the linear PTO produce more electricity. And Fig.20 shows the power curves of the best three gains for both linear PTO damping and nonlinear PTO damping. And it can be concluded that the nonlinear damping has better PTO stability, better gain applicability though it does not show much advantage on the increase of power amount.

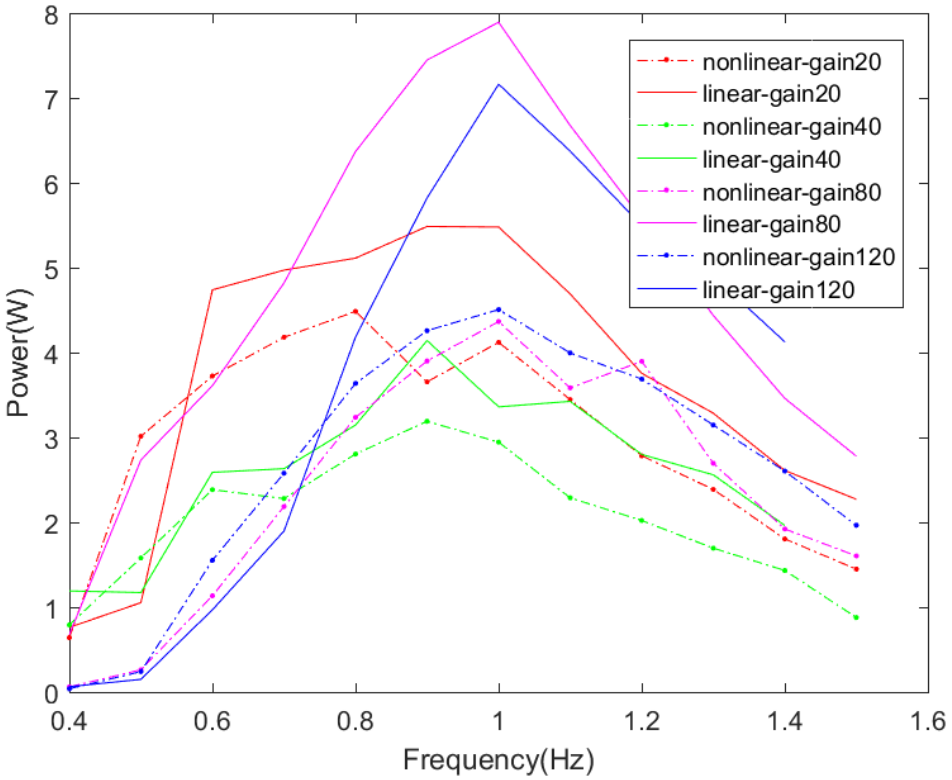

Figure 19 Power comparison of the same gains for linear damping and nonlinear damping

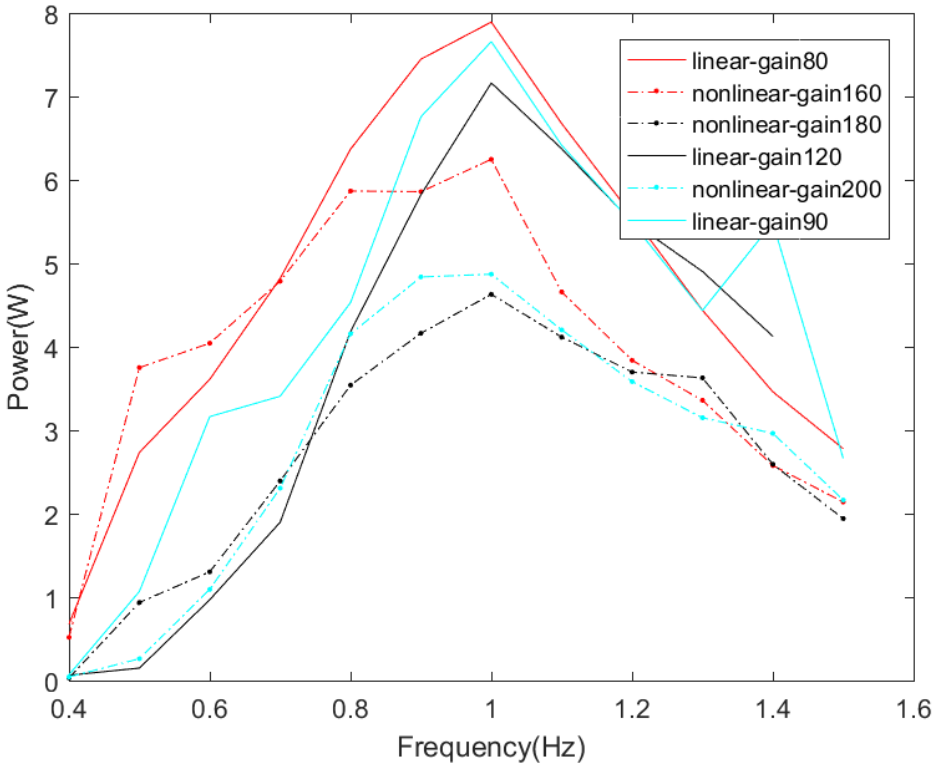

Figure 20 Power comparison of the best three curves for linear damping and nonlinear damping

4.2 Comparison between power curves for the JONSWAP spectrum and user-defined spectrum

Similar in[45, 46], in order to have further insight into the behaviour of the output electricity and explore more possibility in the ocean, apart from the classic JONSWAP spectrum, a series of user-defined spectrum as shown in Fig.21, are used to describe a possible energy spectrum of in the real ocean, proving the feasibility of the PTO simulator. And the power curves are also obtained by the same methods, which are shown in Fig.22. It is obvious that this spectrum produces much less electricity than the JONSWAP spectrum. But the conclusions drawn from section2.3.2 are further validated, that the nonlinear damping has no obvious advantage in the term of the power of output electricity power but have better gain applicability and system stability.

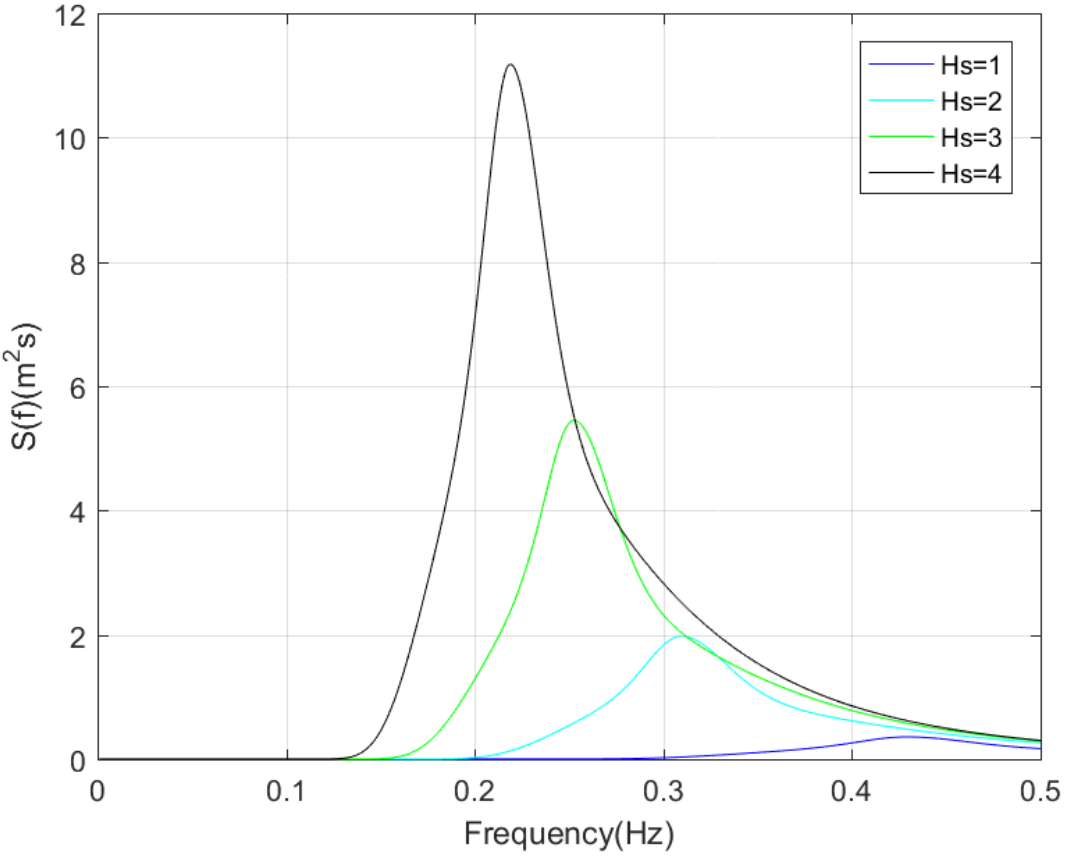

421

422 **Figure 21 User-defined spectrum**

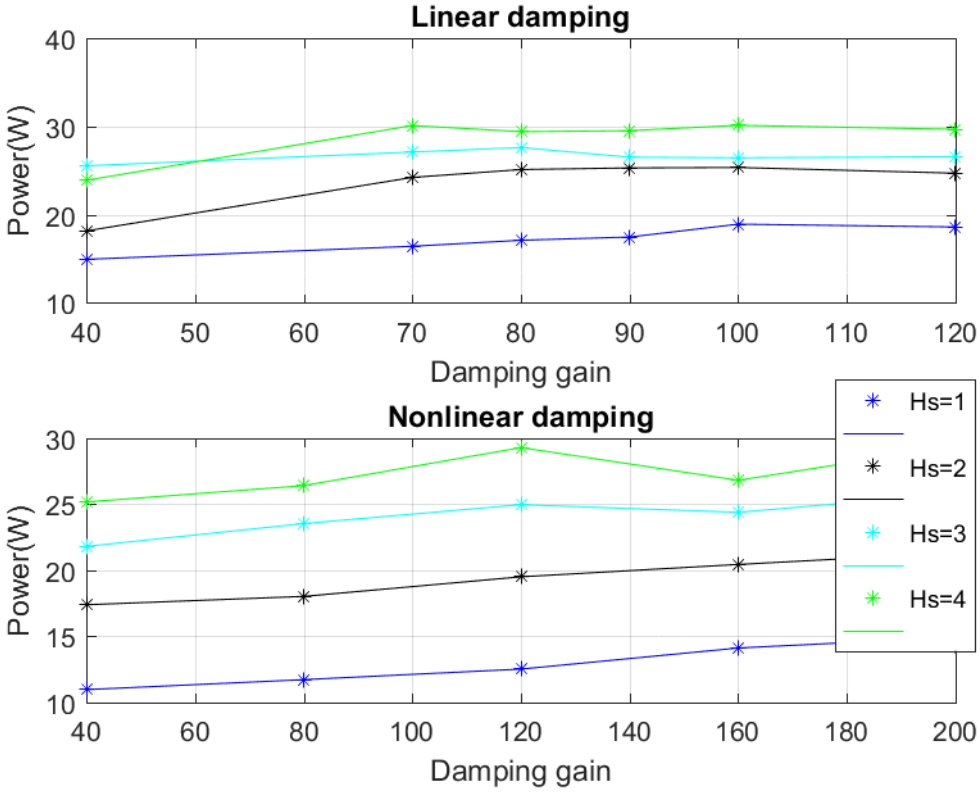

423

Figure 22 Power curves for different wave heights, linear damping, non-linear damping in JONSWAP spectrum

Compare to Fig.15, Fig.22 shows a narrower gain range no matter in linear damping cases or nonlinear damping cases so that it can be seen as a zoom-in plotting. For linear damping when the significant wave heights are 1m and 2m, the electricity production increases smoothly as the gain increases and reaches at a maximum when the gain is 100, then keeps stable. However, when the significant wave heights are 3m and 4m, the output electricity fluctuates to the maximum where the gain is also 100. And the distance between different power curves is small and unequal. For nonlinear damping, the 1m power curve and 2m power curve seem to increase more smoothly than linear damping and reach the maximum at gain180. However, the 3m power curve and 4m power curve reach at the maximum at gain200 or later, the distance between different power curves are more obvious and tend to be equal.

Conclusions

Based on the different damping modes available in the experimental PTO simulation platform, quite some varying PTO strategies are simplified as the PTO damping, and they are simulated to be applied to an OWSC model device. And quite some corresponding tank tests are carried out, and a series of output electricity power curves are obtained by MATLAB data processing methods.

Base on the experimental data, some conclusion have been drawn:

- The best output damping coefficient for linear damping in regular waves is gain 80.
- The best output damping coefficient for nonlinear damping in regular waves is gain 160.
- The comparison of power efficiency under nonlinear PTO damping and linear damping shows that nonlinear PTOs have no distinct advantage in the amount of electricity output, but have better stability and broader damping range.
- Hydrodynamic performance analyses in term of the phase difference are presented, which indicates the OWSC is entirely submissive to waves and the phase control may be that effective as others.
- The power efficiency in the JONSWAP spectrum under different water parameters is drawn.
- Comparison of the output power in different wave spectrum has been carried out, indicating the approach to a full range of ocean possibility. And the electricity output power in JONSWAP spectrum is found to be (approximately 300%) higher than in user-defined frequency for the same wave parameters.

Acknowledgements

The authors acknowledge the China Scholarship Council (No.201606320223) and University of Strathclyde Research Studentship for their financially supporting Xue Jiang's PhD research. The support from the hydrodynamic lab of the University of Strathclyde is also highly appreciated.

Reference

[1] D. I. Forehand, A. E. Kiprakis, A. J. Nambiar, and A. R. Wallace, "A fully coupled wave-to-wire model of an array of wave energy

converters," *IEEE Transactions on Sustainable Energy*, vol. 7, pp. 118-128, 2016.
[2] S. Enger, M. Perić, and H. Monteiro, "Coupling of 3D Numerical Solution Method Based on Navier-Stokes Equations With Solutions Based on Simpler Theories," ed: CILAMCE, 2014.
[3] U. Şentürk and A. Özdamar, "An alternative approach to estimate the hydrodynamic efficiency of an oscillating water column using computational fluid dynamics," *Progress in Computational Fluid Dynamics, an International Journal*, vol. 13, pp. 120-129, 2013.
[4] U. Şentürk and A. Özdamar, "Modelling the interaction between water waves and the oscillating water column wave energy device," *Mathematical and computational applications*, vol. 16, pp. 630-640, 2011.
[5] S. Lin, J. Chen, N. Liang, and Y. Chen, "A study on wave-induced artificial upwelling," *Marine Technology Society Journal*, vol. 50, pp. 48-55, 2016.
[6] M. E. McCormick, *Ocean wave energy conversion*: Courier Corporation, 2013.
[7] J. Falnes, "A review of wave-energy extraction," *Marine Structures*, vol. 20, pp. 185-201, 2007.
[8] F. d. O. Antonio, "Wave energy utilization: A review of the technologies," *Renewable and sustainable energy reviews*, vol. 14, pp. 899-918, 2010.
[9] S. Barstow, G. Mørk, D. Mollison, and J. Cruz, "The Wave Energy Resource," in *Ocean Wave Energy: Current Status and Future Prespectives*, J. Cruz, Ed., ed Berlin, Heidelberg: Springer Berlin Heidelberg, 2008, pp. 93-132.
[10] M. Lehmann, F. Karimpour, C. A. Goudey, P. T. Jacobson, and M.-R. Alam, "Ocean wave energy in the United States: Current status and future perspectives," *Renewable and Sustainable Energy Reviews*, vol. 74, pp. 1300-1313, 2017/07/01/ 2017.
[11] F. He, Z. Huang, and A. W.-K. Law, "An experimental study of a floating breakwater with asymmetric pneumatic chambers for

wave energy extraction," *Applied energy*, vol. 106, pp. 222-231, 2013.
[12] F. He, M. Li, and Z. Huang, "An experimental study of pile-supported OWC-type breakwaters: energy extraction and vortex-induced energy loss," *Energies*, vol. 9, p. 540, 2016.
[13] F. He and Z. Huang, "Characteristics of orifices for modeling nonlinear power take-off in wave-flume tests of oscillating water column devices," *Journal of Zhejiang University-SCIENCE A*, vol. 18, pp. 329-345, 2017.
[14] A. Babarit, "A database of capture width ratio of wave energy converters," *Renewable Energy*, vol. 80, pp. 610-628, 2015.
[15] A. Henry, K. Doherty, L. Cameron, T. Whittaker, and R. Doherty, "Advances in the design of the Oyster wave energy converter," in *RINA Marine and Offshore Energy Conference*, 2010.
[16] Y. Hong, R. Waters, C. Boström, M. Eriksson, J. Engström, and M. Leijon, "Review on electrical control strategies for wave energy converting systems," *Renewable and Sustainable Energy Reviews*, vol. 31, pp. 329-342, 2014.
[17] J. Hals, J. Falnes, and T. Moan, "A comparison of selected strategies for adaptive control of wave energy converters," *Journal of Offshore Mechanics and Arctic Engineering*, vol. 133, p. 031101, 2011.
[18] T. Battisti, G. Faruolo, and L. Magliocchetti, "A State-of-the-Art SWIL (Software in the Loop) Electronic Warfare System Simulator for Performance Prediction and Validation," in *International Workshop on Modelling and Simulation for Autonomous Systems*, 2015, pp. 154-164.
[19] J. Henriques, R. Gomes, L. Gato, A. Falcão, E. Robles, and S. Ceballos, "Testing and control of a power take-off system for an oscillating-water-column wave energy converter," *Renewable Energy*, vol. 85, pp. 714-724, 2016.
[20] J. Chen, C. Xu, Y. Chen, J. Ji, and D. Yan, "Study of a Novel Underwater Cable With Whole Cable Monitoring," *Marine Technology Society Journal*, vol. 50, pp. 75-82, 2016.

[21] J. Chen, H. Zhu, L. Zhang, and Y. Sun, "Research on fuzzy control of path tracking for underwater vehicle based on genetic algorithm optimization," *Ocean Engineering*, vol. 156, pp. 217-223, 2018.
[22] S. Dai, "Assessing the performance of an oscillating water column type wave energy device," University of Strathclyde, 2016.
[23] Z. Zang, Q. Zhang, Y. Qi, and X. Fu, "Hydrodynamic responses and efficiency analyses of a heaving-buoy wave energy converter with PTO damping in regular and irregular waves," *Renewable Energy*, vol. 116, pp. 527-542, 2018.
[24] B. Drew, A. R. Plummer, and M. N. Sahinkaya, "A review of wave energy converter technology," ed: Sage Publications Sage UK: London, England, 2009.
[25] A. Henry, P. Schmitt, T. Whittaker, A. Rafiee, and F. Dias, "The characteristics of wave impacts on an oscillating wave surge converter," in *The Twenty-third International Offshore and Polar Engineering Conference*, 2013.
[26] E. Renzi and F. Dias, "Hydrodynamics of the oscillating wave surge converter in the open ocean," *European Journal of Mechanics-B/Fluids*, vol. 41, pp. 1-10, 2013.
[27] T. Whittaker, D. Collier, M. Folley, M. Osterried, A. Henry, and M. Crowley, "The development of Oyster—a shallow water surging wave energy converter," in *Proceedings of the 7th European Wave and Tidal Energy Conference, Porto, Portugal*, 2007, pp. 11-14.
[28] S. D. Xue Jiang , David Clelland, "An innovative generic platform to simulate real-time PTO damping forces for ocean energy converters based on SIL method," ed.
[29] T. Whittaker and M. Folley, "Nearshore oscillating wave surge converters and," 2011.
[30] A. G. Piersol and C. M. Harris, *Harri's Shock and Vibration Handbook Fifth Edition*: Mcgraw-hill, 2017.
[31] M. Li, "Three classes of fractional oscillators," *Symmetry*, vol. 10, p. 40, 2018.

[32] M. Li, "Fractal time series—a tutorial review," *Mathematical Problems in Engineering*, vol. 2010, 2010.
[33] Y.-B. He, J.-X. Luo, X.-D. Li, Z.-Z. Gao, and Z. Wen, "Evidence of internal-wave and internal-tide deposits in the Middle Ordovician Xujiajuan Formation of the Xiangshan Group, Ningxia, China," *Geo-Marine Letters*, vol. 31, pp. 509-523, 2011.
[34] L. Li, Y. Gao, Z. Yuan, S. Day, and Z. Hu, "Dynamic response and power production of a floating integrated wind, wave and tidal energy system," *Renewable Energy*, vol. 116, pp. 412-422, 2018/02/01/ 2018.
[35] M. J. Muliawan, M. Karimirad, and T. Moan, "Dynamic response and power performance of a combined Spar-type floating wind turbine and coaxial floating wave energy converter," *Renewable Energy*, vol. 50, pp. 47-57, 2013/02/01/ 2013.
[36] Z. Zang, Q. Zhang, Y. Qi, and X. Fu, "Hydrodynamic responses and efficiency analyses of a heaving-buoy wave energy converter with PTO damping in regular and irregular waves," *Renewable Energy*, vol. 116, pp. 527-542, 2018/02/01/ 2018.
[37] C. Stansberg, G. Contento, S. W. Hong, M. Irani, S. Ishida, R. Mercier, *et al.*, "The specialist committee on waves final report and recommendations to the 23rd ITTC," *Proceedings of the 23rd ITTC*, vol. 2, pp. 505-551, 2002.
[38] M. Li, "A method for requiring block size for spectrum measurement of ocean surface waves," *IEEE Transactions on Instrumentation and Measurement*, vol. 55, pp. 2207-2215, 2006.
[39] J.-B. Saulnier, A. Clément, F. d. O. António, T. Pontes, M. Prevosto, and P. Ricci, "Wave groupiness and spectral bandwidth as relevant parameters for the performance assessment of wave energy converters," *Ocean Engineering*, vol. 38, pp. 130-147, 2011.
[40] S. Parmeggiani, J. P. Kofoed, and E. Friis-Madsen, "Extreme loads on the mooring lines and survivability mode for the wave dragon wave energy converter," in *World Renewable Energy*

Congress-Sweden; 8-13 May; 2011; Linköping; Sweden, 2011, pp. 2159-2166.

[41] R. Pascal and I. Bryden, "Directional spectrum methods for deterministic waves," *Ocean Engineering*, vol. 38, pp. 1382-1396, 2011.

[42] Y.-H. Yu and Y. Li, "A RANS simulation of the heave response of a two-body floating-point wave absorber," in *The Twenty-first International Offshore and Polar Engineering Conference*, 2011.

[43] P. Troch, C. Beels, J. De Rouck, and G. De Backer, "Wake effects behind a farm of wave energy converters for irregular long-crested and short-crested waves," *Coastal Engineering Proceedings*, vol. 1, p. 53, 2011.

[44] L. Rusu and F. Onea, "Assessment of the performances of various wave energy converters along the European continental coasts," *Energy*, vol. 82, pp. 889-904, 2015.

[45] Q. Guo and Z. Xu, "Simulation of deep-water waves based on JONSWAP spectrum and realization by MATLAB," in *Geoinformatics, 2011 19th International Conference on*, 2011, pp. 1-4.

[46] G. Kim, W. M. Jeong, K. S. Lee, K. Jun, and M. E. Lee, "Offshore and nearshore wave energy assessment around the Korean Peninsula," *Energy*, vol. 36, pp. 1460-1469, 2011.

List of equations

List of figures

List of table